2023-11-01

The impact of sediment flux and calibre on flood risk in the Kathmandu Valley, Nepal

Thapa, S

10.1002/esp.5731
Earth Surface Processes and Landforms
Wiley

The impact of sediment flux and calibre on flood risk in the Kathmandu Valley, Nepal

Saraswati Thapa[1,2,*], Hugh D. Sinclair[1], Maggie J. Creed[3], Simon M. Mudd[1], Mikael Attal[1], Alistair G. L. Borthwick[4,5], Bhola N. Ghimire[2], and C. Scott Watson[6]

[1]School of Geosciences, University of Edinburgh, Drummond Street, Edinburgh, EH8 9XP, UK
[2]Pulchowk Campus, Institute of Engineering, Tribhuvan University, Lalitpur, Nepal
[3]James Watt School of Engineering, University of Glasgow, Glasgow G12 8QQ, UK
[4]School of Engineering, University of Edinburgh, Kings Buildings, Edinburgh, UK EH9 3FB
[5]University of Plymouth, Plymouth, PL4 8AA, UK
[6]COMET, School of Earth and Environment, University of Leeds, Leeds, West Yorkshire, LS2 9JT, UK
[*]Correspondence to: Saraswati Thapa, School of Geosciences, University of Edinburgh, Drummond Street, Edinburgh, EH8 9XP, UK. E-mail: Saraswati.Thapa@ed.ac.uk

October 3, 2023

Abstract

This paper investigates how variations in sediment supply, grain size distribution, and climate change affect channel morphology and flood inundation in the Nakkhu River, Kathmandu, Nepal. Climate change-induced extreme rainfall is expected to increase flood intensity and frequency, causing severe flooding in the Kathmandu basin. The upper reaches of the Nakkhu River are susceptible to landslides and have been impacted by large-scale sand-mining. We simulate potential erosion and deposition scenarios along a 14 km reach of the Nakkhu River using the landscape evolution model CAESAR-Lisflood with a 10 m digital elevation model, field-derived sediment grain size data, daily discharge records, and flood forecast models. In a series of numerical experiments, we compare riverbed profiles, cross-sections, flood extent, and flow depths for three scenarios (1.2-, 85-, and 1000-year return period floods). For each scenario, the model is first run without sediment transport and then with sediment transport for three grain size distributions (GSDs) (observed average, finer and coarser). In all cases, the inclusion of sediment led to predicted floods of a larger extent than estimated without sediment. The sediment grain size distribution was found to have a significant influence on predicted river morphology and flood inundation, especially for lower magnitude, higher probability flood

events. The results emphasise the importance of including sediment transport in hydrological models when predicting flood inundation in sediment-rich rivers such as those in and around the Himalaya.

Keywords: River morphology; Sediment transport; Grain size distribution; Climate change; Flood modelling; Nepal

1 Introduction

River floods are well-established agents of disasters whose socio-economic consequences can include loss of life, reduction in societal well-being, and damage to property and infrastructure (UNDRR, 2020). The impact of flooding is expected to escalate due to increasing urbanization and the effects of climate change (IPCC, 2007; Masson-Delmotte et al., 2021). In Nepal, the impact of flooding is influenced by a range of factors, including climate change, land use, and anthropogenic activities (e.g., urbanisation) (Dhital and Kayastha, 2013; Basnyat et al., 2020). One of the major causes of flooding in Nepal is the effect of continuous heavy rainfall during the monsoon; approximately 80% of the annual rainfall occurs from June to September (Dahal and Hasegawa, 2008; Dhital and Kayastha, 2013; Dewan, 2015). In addition, in steep mountain regions, unstable upland hillsides cause rock falls and landslides which result in temporary damming of rivers, eventually leading to extreme floods due to landslide-dam outbursts (Shrestha and Nakagawa, 2016; Ruiz-Villanueva et al., 2017; Gurung et al., 2021). These extreme flash floods and lake outburst floods can overwhelm flood-protection works, causing river embankments and dams to fail, increasing flood inundation (Chakraborty et al., 2010).

Recent studies based on field observations and model predictions confirm that morphological changes after an extreme flood event can have major repercussions on subsequent river flow dynamics and flood inundation (Stover and Montgomery, 2001; Pinter and Heine, 2005; Lane et al., 2007; Neuhold et al., 2009; Slater et al., 2015; Guan et al., 2015; Fieman et al., 2020; Milan and Schwendel, 2021). High-magnitude, short-duration floods can cause significant erosion in upstream reaches before depositing sediment in the channel and on the floodplains of downstream reaches, rapidly modifying the local geomorphology (Turowski et al., 2009; Yager et al., 2012; Attal, 2017; Fieman et al., 2020). Flood-induced geomorphological processes such as sediment delivery and in-channel sedimentation influence future inundation risk because of changes to bed elevation and channel geometry which then alter the water conveyance capacity of the channel (Stover and Montgomery, 2001; Lane et al., 2007; Slater et al., 2015; Fieman et al., 2020). Consequently, to develop accurate flood risk assessments and flood management processes, it is important to understand the relationship between flood events and morphological evolution (Coulthard et al., 2002; Guan et al., 2015).

In mountain catchments, river morphology is sensitive to variations in sediment supply owing to the close connection between hillslope sediment supply and channel evolution. In addition to the natural processes affecting sediment transport such as major storms, landslides and debris flows (Dingle et al., 2020), human activities such as sand mining, dam construction, and river encroachment by embankments and flood walls can alter fluvial sediment dynamics (Chakraborty et al., 2010). Given the complexity of water-sediment processes, it is difficult to isolate the effect of each driver (Van De Wiel and Coulthard, 2010). Analysis of the impact of multiple independent parameters on channel migration and sediment transport in floodplains is particularly challenging (O'Connor et al., 2003). Numerical models offer the opportunity to integrate these processes at catchment scale to provide insight into complex water-sediment interactions (Feeney et al., 2020; Owens and Collins, 2006).

In Nepal, flood simulation for hazard assessment is usually based on static digital elevation models (DEMs)(Dingle et al., 2020) and on assumptions of clear water and a fixed bed (Thapa

et al., 2020), therefore neglecting the effect of flood-induced geomorphological change (Guan et al., 2016). Older DEMs, such as Shuttle Radar Topography Mission (SRTM) collected in February 2000 (Farr et al., 2007), have limited utility in defining channels in the Himalayas, where channels may have migrated several DEM pixels since the original data were acquired (Dingle et al., 2020). When combined with hydraulic modelling that neglects sediment transport, the reliability and use of DEMs become questionable for understanding sediment-laden river systems (Coulthard et al., 1997; Dingle et al., 2020). There is a clear need to explore the role of sediment transport and grain size variability on flooding; coupled hydraulic-sediment transport models or landscape evolution models (LEMs) can be useful in this regard.

Over the past 15 years, substantial advances have been made in LEMs (Coulthard and Wiel, 2006; Van De Wiel et al., 2007; Coulthard et al., 2007; Temme et al., 2011; Van De Wiel et al., 2011; Coulthard et al., 2013). Even so, LEM-based assessments for flood impact analysis are often limited by a lack of available field data for model calibration and validation. Sensitivity analysis of model parameters is therefore important while setting up the initial LEM (Hancock, 2009, 2012; Temme et al., 2011; Ziliani et al., 2013; Skinner et al., 2018; Wong et al., 2021; Skinner and Coulthard, 2023). Hancock (2009) demonstrated that the CAESAR LEM is very sensitive to input parameters, especially sediment particle size distribution and determination of the hydrological and erosion parameters for sediment transport prediction. The models are affected by the choice of equations, particularly empirical closure relations for sediment transport. For example, the CAESAR-Lisflood (C-L) model (Coulthard et al., 2013), the CAESAR LEM model (Coulthard et al., 2002) integrated with the Lisflood-FP 2D hydrodynamic model (Bates and De Roo, 2000; Bates et al., 2010), offers a choice of three approaches for calculating sediment transport: the Meyer-Peter and Müller (1948) empirical formula for moderate transport rates of gravel, the Einstein (1950) statistical method for sandy rivers, and the Wilcock and Crowe (2003) empirical approach derived from mixed gravel and sand tests that gives accurate predictions of transient bed armouring aggradation and degradation. The CAESAR LEM or integrated CAESAR-Lisflood models both use a digital elevation model to define topography and have been applied to simulate land evolution scenarios for many parts of the world (Coulthard and Macklin, 2001, 2003; Coulthard et al., 2002, 2005; Van De Wiel et al., 2007; Hancock, 2009; Coulthard and Van De Wiel, 2013, 2017; Liu and Coulthard, 2017; Skinner et al., 2018; Feeney et al., 2020; Ramirez et al., 2020; Ziliani et al., 2020; Wong et al., 2021; Ramirez et al., 2022; Skinner and Coulthard, 2023). Recently, Skinner et al. (2018) carried out a sensitivity analysis of the C-L (v1.8f) model using 50 m and 10 m DEMs for the Swale catchment, UK (a temperate, perennial medium-sized catchment with an area of 181 km^2), and the Tin Camp Creek catchment, Australia (a tropical, ephemeral small catchment with an area of 0.5 km^2) considering bedload only (without using suspended sediment processes in the model). Skinner et al. (2018) tuned their model to 15 different parameters and found that the greatest uncertainty arose from the choice of sediment transport formula. In addition, parameter sensitivity was also strongly influenced by DEM resolution. Skinner et al. (2018) also recommended examining the effects of grain-size distribution, lateral erosion, and Manning roughness coefficient on predicted flood inundation.

We use the CAESAR-Lisflood (v1.9j) model to investigate the effect of variations in sediment grain size distribution on flood events along a 14 km reach of the Nakkhu River, the largest southern tributary in the Kathmandu basin, Nepal. The main channel of the Nakkhu River is highly mobile, and thus susceptible to bank erosion, downcutting, and accumulation of bar forms (Maharjan and Tamrakar, 2010). These processes are heightened during extreme flood events, as observed in river geometric surveys, satellite images from Sentinel-2 Normalised Difference Suspended Sediment Index (NDSSI) data set [1] and Google Earth imagery that show that the 15 m wide river channel has migrated several river widths since 2003.

The Nakkhu River is of particular interest because it is located in a rapidly urbanising

[1] https://apps.sentinel-hub.com/eo-browser

region of the Kathmandu Valley and carries a large amount of sediment from active landslides and quarrying and mining activities upstream. The rapid urbanisation has not only led to an increase in gravel and sand mining of the river but also increased levels of construction along the riverbanks and floodplains. In the past (1960s and 1980s, see the Department of Hydrology and Meteorology, Nepal (DHM)[2] discharge record), the Nakkhu has also been affected by landslide dam breaches in the upstream section of the river, leading to high water levels downstream. These natural and anthropogenic impacts affect river morphology and grain size distribution, making the Nakkhu River an interesting case study for our analysis. This study will highlight the importance of sediment transport in the context of flood risk in Himalayan rivers with high sediment flux.

Sensitivity analyses are undertaken to assess the influence of lateral bank erosion parameters, Manning roughness and sediment grain-size distribution. The impact of different annual peak flood events is explored through scenario tests. We address: (1) the influence of sediment grain-size distribution on fluvial morphology; and (2) how changes in channel geometry driven by sediment transport translate into inundation for different scenarios including extreme future floods promoted by climate change. To the authors' knowledge, the paper describes the first application of an LEM incorporating calibrated sediment transport with historical and future flood scenarios to a Himalayan river system.

2 Methods

2.1 Study area

The Nakkhu River is located within the Kathmandu basin in central Nepal. It initially flows westward from the south-east corner of the basin before turning northward until it joins the Bagmati River as one of the river's seven major tributaries (Figure 1). It is 26 km long and has a watershed area of 58 km^2. The Nakkhu River is steep and highly energetic, carrying a large amount of sediment during the monsoon season (Maharjan and Tamrakar, 2010). As a result, the Nakkhu River has an unstable channel morphology, with widespread bank erosion and deposition. According to Maharjan and Tamrakar (2010), the estimated bankful water discharge for a flood event in 2011 was from 2.97 $m^3\ s^{-1}$ to 10.24 $m^3\ s^{-1}$ along the river. The subsequent survey of February 2021 suggests that the bankful discharge varied spatially from 50 $m^3\ s^{-1}$ to 120 $m^3\ s^{-1}$ by river channel migration and morphology change. Even though the rivers have great cultural significance in Nepal, the Nakkhu River has been adversely impacted by pollution from raw domestic sewage, sediment extraction, bank encroachment, and dumping of quarry waste (Maharjan and Tamrakar, 2010, 2011). Like many Himlalayan rivers, the Nakkhu River also experiences extraction of specific grain sizes of sediment through sand and gravel mining (GoN, 2008; Stoffel et al., 2016; Maharjan and Tamrakar, 2010).

2.2 Model overview and data sources

We used the CAESAR-Lisflood (Version 1.9j)[3] landscape evolution model (LEM) (Coulthard et al., 2013) to simulate water and sediment discharges throughout a 14-km reach of the Nakkhu River between the Tikabhairav gauging station (blue square Figure 1) to the Nakkhu-Bagmati confluence. Reach-based and catchment-based versions of CAESAR-Lisflood have been successfully applied to predictions of short-term extreme geomorphology and long-term land-form evolution in many basins worldwide (Coulthard et al., 2013; Feeney et al., 2020; Fieman et al., 2020; Ramirez et al., 2020). Of the three sediment transport options in CAESAR-Lisflood, we selected the Wilcock and Crowe (2003) formula because it was most representative of the

[2] http://hydrology.gov.np

[3] https://sourceforge.net/p/caesar-lisflood/wiki/Home/

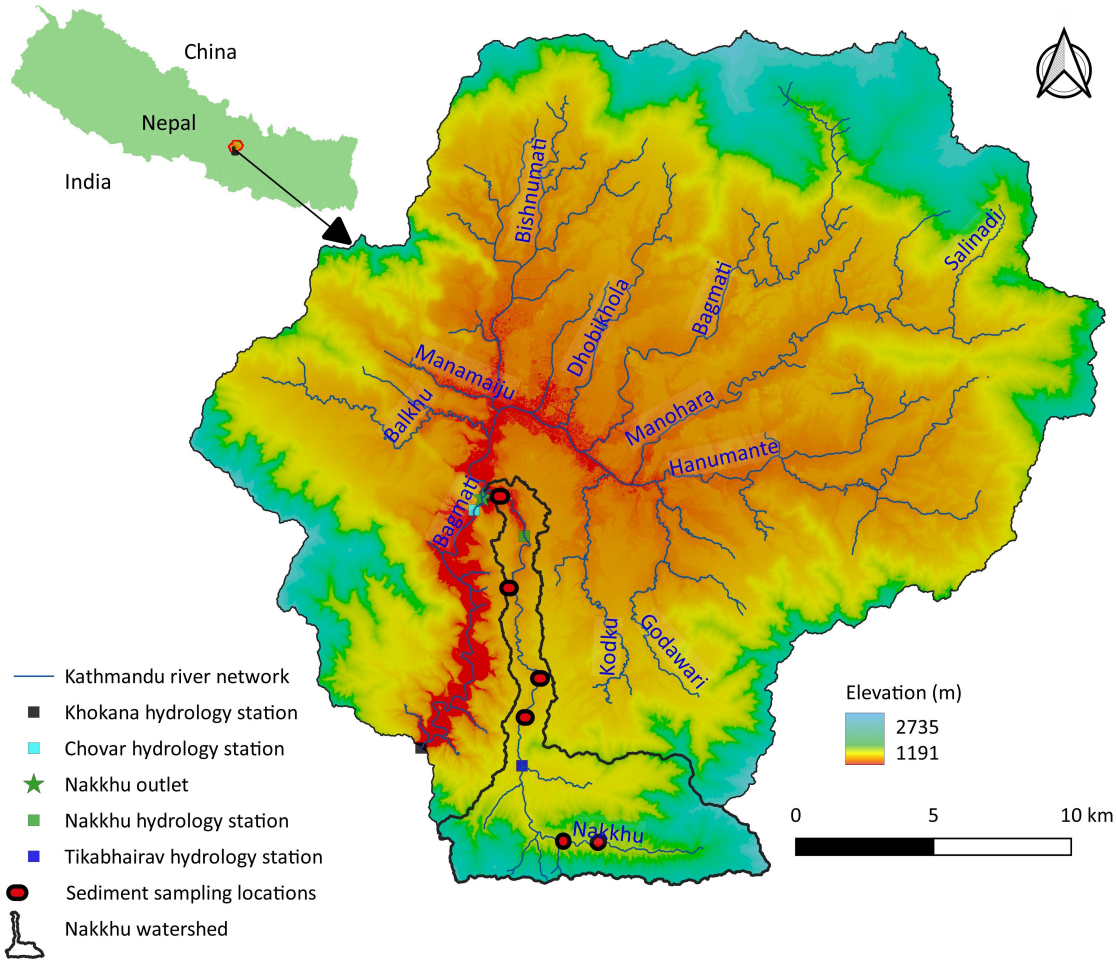

Figure 1: Kathmandu basin extracted upstream of Khokana hydrological station on the Bagmati River, including the Nakkhu River watershed (solid black line) and sediment sampling sites (red dots).

mixed grain size distribution in the Nakkhu basin (see the section '2.3 Model spin-up'); it was designed to account for multiple grain size fractions and incorporates changes in entrainment thresholds linked to processes such as armouring. The model incorporates multiple grain size distributions, as well as selective erosion, transport, and deposition of distinct size fractions. Key data inputs for the C-L model include a digital elevation model (DEM), hydraulic data, and sediment grain size distribution (GSD) data. These data and the strategy for the modelling are described in the following sections.

2.2.1 Digital Elevation Model

The DEM was constructed from tri-stereo Pleiades satellite images obtained on the 25^{th} of December 2019 and 13^{th} January 2020, a commercial data-set that was made available for research use. IDs of the images used to make the DEM are provided in the supplementary document S1. The panchromatic band (0.5 m resolution) was processed using rational polynomial coefficients (RPCs) in Agisoft Metashape v1.8.4 to create a 2 m resolution DEM. The DEM was then resampled to 10 m resolution. Due to the constraints of the CAESAR-Lisflood model[4], which is best suited to a DEM with 0.25 to 0.5 million pixels, or a maximum of 2 million pixels, the DEM was resampled to 10 m resolution. At 10 m resolution the study area DEM has 301035 pixels, compared to 7.5 million pixels at 2 m resolution. Although the model results may be

[4] https://sourceforge.net/p/caesar-lisflood/wiki/Instructions/

sensitive to DEM resolution (Temme et al., 2011; Skinner et al., 2018; Skinner and Coulthard, 2023), it was not possible to run models of this river reach with the original DEM pixel size using CAESAR-Lisflood. For more than 2 million grid cells, a high-performance computing system can be helpful, as such implemented in the HAIL-CAESAR model (High-performance Architecture Independent Lisflood-CAESAR model)[5] suggested by Valters (2017) and the C-L model (Coulthard et al., 2013). We found the 2 m and resampled 10 m DEMs produced river longitudinal profiles consistent with ground-based topographic survey data of the Nakkhu River obtained in November 2018, for the Bagmati Corridor Development Project by the Nepal Government. The profiles were compared by computing the root-mean-square errors which are 0.906 and 0.932 m, respectively, for the 2 m and 10 m DEMs. A comparison between the 2 m and 10 m DEMs was made at various locations, and we have included results for four locations: L3, L4, L5, and L6 (Figure 2b) in the supplementary Figure S1. The modelled DEM extends from Tikabhairav (Figure 2) down to the confluence between the Nakkhu and Bagmati rivers.

2.2.2 Hydraulic input data

Flow stage and discharge data, observed across different time periods, were obtained from the Department of Hydrology and Meteorology, Nepal for Tikabhairav (1963-1980), Nakkhu (2018), Chovar (1963-1980), and Khokana (1992-2020) stations (Figure 1). The Tikabhairav station is located at the upstream end of the study reach. The Nakkhu station is located in the downstream part of the study site, where the Nakkhu Valley opens up over a wide floodplain where urban development is occurring at a rapid pace; the Chovar and Khokana stations are located on the Bagmati River about 0.5 km and 10 km downstream of the Nakkhu-Bagmati confluence (Figure 1). Due to the limited discharge data available for the Tikabhairav station in the Nakkhu River (1963-1980), we scaled the discharge data from corresponding data at Khokana (1992-2018) using the drainage area ratio method, a widely used method for estimate discharge in ungauged rivers (Emerson et al., 2005; Yilmaz and Onoz, 2020; Marahatta et al., 2021). To validate this process, we used the same scaling method to estimate the discharge at Tikabhairav using data from Chovar (1963-1980). We compared the available observed maximum monthly discharge (1963-1980) at Tikabhairav with the scaled discharge using a linear regression model that showed an R^2 value of 0.717.

Based on this adjusted discharge time series at Tikabhairav, a return period analysis was carried out to estimate return period flood magnitudes up to the 1000-year event (see next section; Figure 3). We used the 2001 flood (estimated 1.5-year) for model spin-up. We then modelled scenarios based on three floods of different return periods to explore the effect of flood intensity on river morphology and inundation: 1.2-year (discharge record of 2006 flood), 85-year (discharge record of the 2002 flood) and 1000-year (predicted) return period flood.

To calculate extreme flow values for the Nakkhu River, we fitted Gumbel, Fréchet, and generalized logistic (GL) distributions as recommended by the Flood Estimation Handbook (IH, 1999) to the adjusted observed annual maximum flow data for the Nakkhu River over 26 years. The plot of peak discharge against return period in Figure 3 shows that the Gumbel distribution (commonly used by flood forecasters in Nepal) and GL distribution give similar fits. The peak flood of 56.4 $m^3\ s^{-1}$ at Nakkhu in 2002 corresponds to return periods of 75, 85, and 18 years for the Gumbel, GL, and Fréchet distributions, respectively (Figure 3). 100-year return period flood discharges are predicted to be 58.2, 59.7 and 126.3 $m^3\ s^{-1}$ from the Gumbel, GL, and Fréchet distributions, respectively. Chi-square goodness-of-fits at 10%, 5%, and 1% significance levels were tested, and it was found that the Gumbel and GL distributions satisfied the ${\chi^2}_{critical} > {\chi^2}_{observation}$ condition. The Fréchet distribution did not satisfy the Chi-square fit. In addition, root-mean-square error (RMSE) statistics indicate that the GL distribution provides the best fit with a minimum RMSE of 3.1 $m^3\ s^{-1}$, whereas for Gumbel the RMSE is

[5] https://hail-caesar.readthedocs.io/en/latest/intro/

3.2 $m^3\ s^{-1}$ and for Fréchet the RMSE is 4.8 $m^3\ s^{-1}$. We therefore use the GL distribution for the future flood forecasts herein. According to the GL distribution, the peak historical flood which occurred in 2002 corresponds to a 1-in-85 year return period, and the peak flood of 2006 (1-in-1.2 year) represents a typical annual flood in the Nakkhu River.

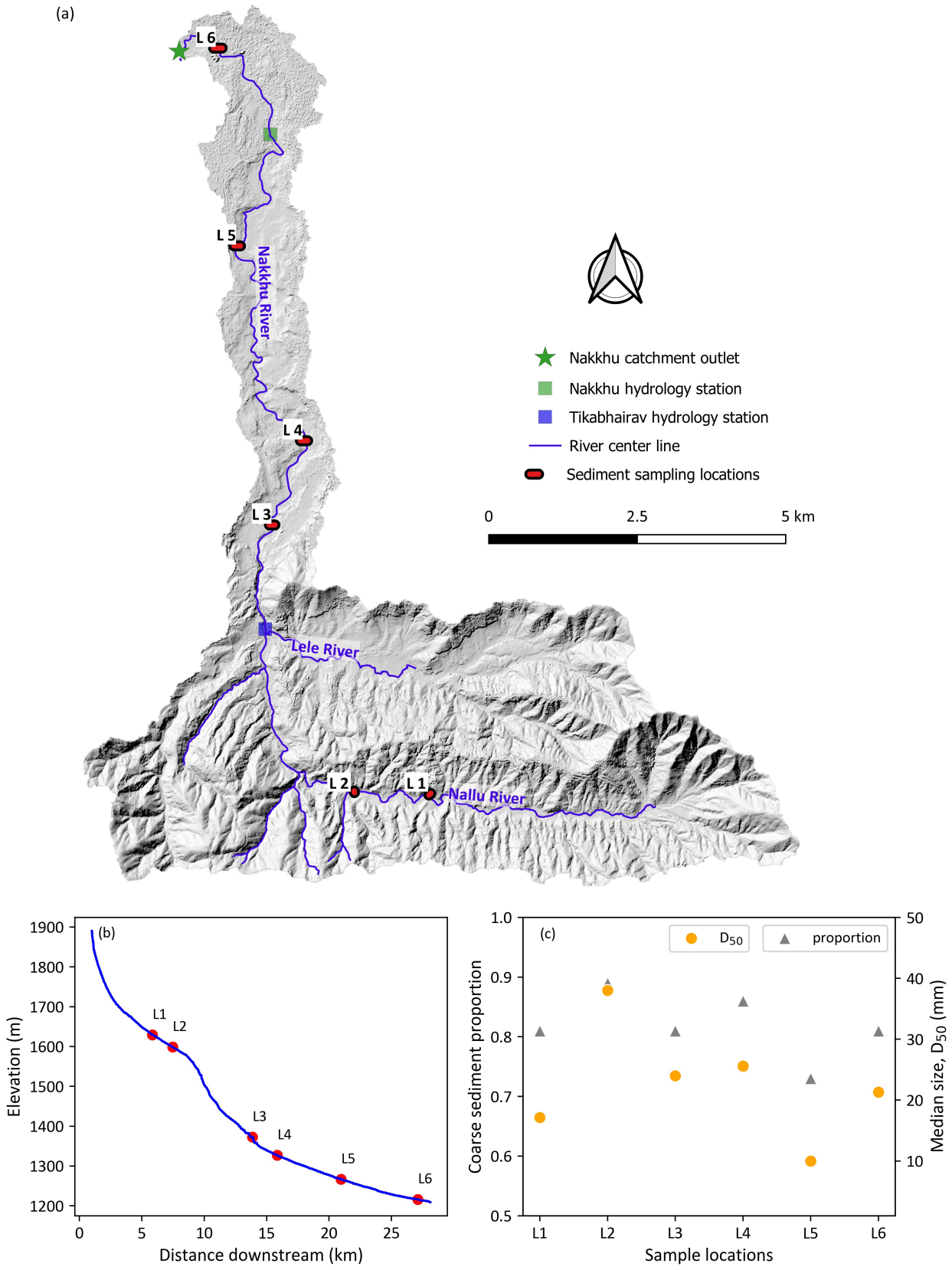

Figure 2: (a) Hillshade of the Nakkhu watershed with sediment sampling locations L1 to L6 marked along the river; (b) river profile with sampling locations indicated; and (c) scatter plot showing proportion of coarse ($D \geq 2$ mm) sediment grain size distribution and median size (D_{50}) of collected samples at different locations after sieving.

To investigate the impact of climate change on flooding and hence river morphology, we identified an extreme flood scenario based on the application of general circulation models

(GCM) to the same basin (Shrestha et al., 2023). Shrestha et al. (2023) report that the present-day 100-year return period rainfall event will be equivalent to a 20- to 25-year return period value in the mid future (2046-2075) for the Bagmati basin. The predicted mid-future 100-year flood in Shretha et al.'s study is approximately equal to the 1000-year return period flood predicted by the GL distribution (95 m^3 s^{-1}) based on the archive data. We therefore investigate the impact of the present day 1000-year discharge as a possible 100-year flood event in the mid-future.

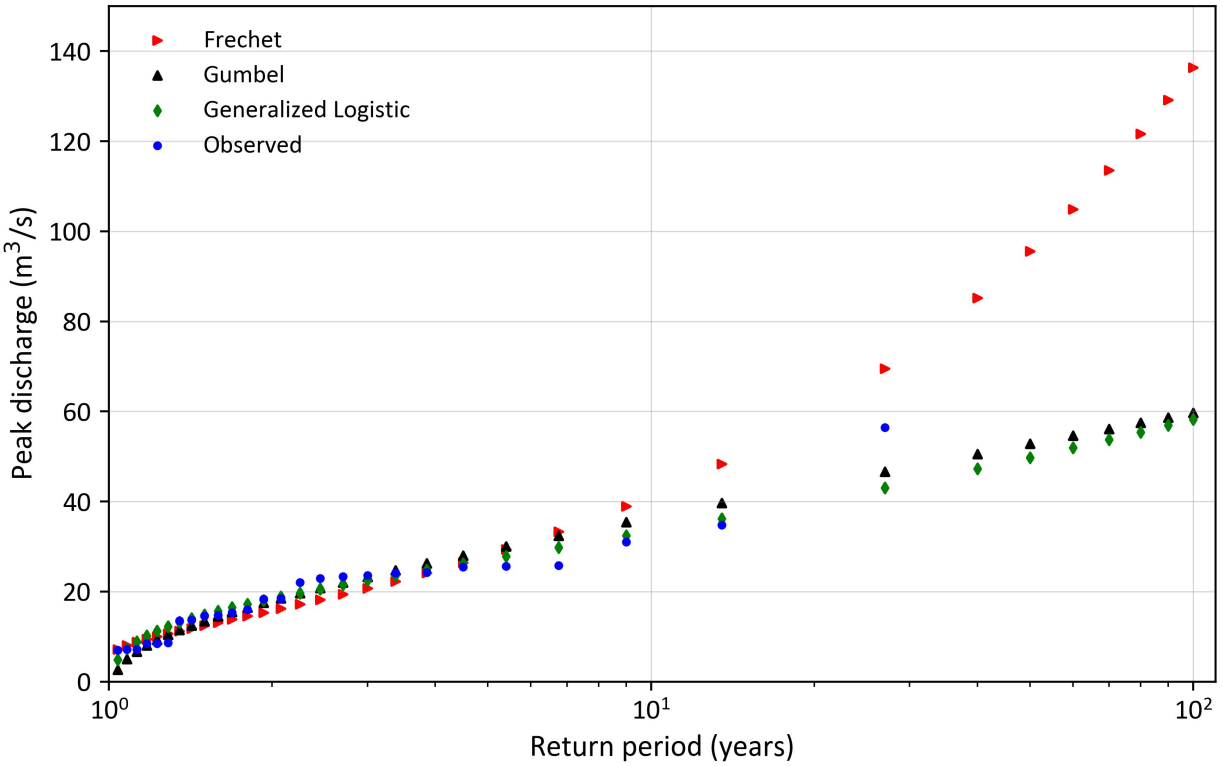

Figure 3: Gumbel, Fréchet and Generalized Logistic flow distributions fitted to the Nakkhu River from observed peak daily discharge data obtained at Khokana hydrological station, Nepal, from 1992 to 2017 inclusive. The Fréchet distribution tends to overestimate the observed data.

2.2.3 Sediment data

Data on suspended sediment concentrations in the Bagmati River at the Khokana station were obtained from the DHM, Nepal. The data mostly included daily measurements taken during the monsoon season, and biweekly data during the pre- and post-monsoon periods from 2003 to 2020, although a few years have missing data records. On analysing the record of suspended sediment concentration data at Khokana from 2010 to 2015, the minimum and maximum concentrations were found to be 7 Parts per million (PPM) to 8193 PPM, respectively. The yearly suspended sediment yield at Khokana from 2010 to 2015 was estimated to range from a minimum of 220 tonnes km^{-2} yr^{-1} recorded in 2015 to a maximum of 1480 tonnes km^{-2} yr^{-1} recorded in 2011. By comparison, Milliman and Meade (1983) report a global average sediment yield of 150–183 tonnes km^{-2} yr^{-1} and a range for large rivers in Asia of 380–543 tonnes km^{-2} yr^{-1}. Field observations of highly turbid water, in particular during the monsoon, caused by landslides and disruption by ongoing sand mining work in the upstream part of the catchment, suggest the Nakkhu River could be a main contributor to the Bagmati river's sediment yield.

We acquired data on suspended sediment concentration and grain size distribution that was originally collected by the Bagmati Hydropower Project which sampled sediment concentration

at a location 23 km downstream of the Bagmati-Nakkhu confluence two or three times a day from June 15 to September 23, 2012. Here, the suspended sediment comprised particles of diameter less than 2 mm with median grain size D_{50} of 0.1 mm, and the suspended sediment concentration ranged from 65 to 14515 PPM.

Maharjan and Tamrakar (2010) used Wolman's point counts on gravel bars to determine the sediment grain size distribution in four segments of the Nakkhu River, and found that the median grain diameter D_{50} was 28 mm at a location 26 km upstream of the confluence of the Nakkhu and Bagmati rivers, and that D_{50} decreased to 0.1 mm in the downstream reach near the confluence. We sampled the sediment on gravel bars at six locations along the Nakkhu River in November 2021 (Figure 2): two upstream and four downstream of Tikabhairav. To measure the grain size distribution of the subsurface sediment on gravel bars, we used the method described by Attal and Lavé (2006) and Dingle et al. (2020). The sampling technique involved excavating 1 m^3 pits on gravel bars after removing the armor layer over the thickness of the largest clast. The grain size distribution of the sediment was determined by sieving and weighing approximately 2600 kg of sediment taken from each gravel bar. Initially, the samples were classified into 13 classes after sieving through 11 sieves of diameters ranging from D = 0.075 mm to 80 mm and manually measuring samples with particle diameter (D) greater than 80 mm. Each sample was reclassified into nine classes to fit those of the C-L model, where the median value of sieve size represents the class interval. All six samples exhibited a wide and bimodal distribution (10 mm $< D_{50} <$ 37 mm) with peaks at 1 mm and 32 mm. The wide range of grain sizes is a specific characteristic of the Nakkhu River which is shorter (26 km) and steeper than the other tributaries of the Kathmandu basin. We found little variation between samples L3 to L6 (Figure 2c). Due to the lack of a clear downstream trend in observed grain size distribution (Figure 2c), we agglomerated the distributions from the four locations of the modelled reach (L3 to L6, Figure 2) into one grain size distribution representative of the Nakkhu River sediment in this part of the reach, herein referred to as the observed average distribution (Figure 4a). Within our grain size distributions, we classify fine sand for particles of diameter less than 2 mm, and coarse gravel otherwise (coarse proportion shown in Figure 2c).

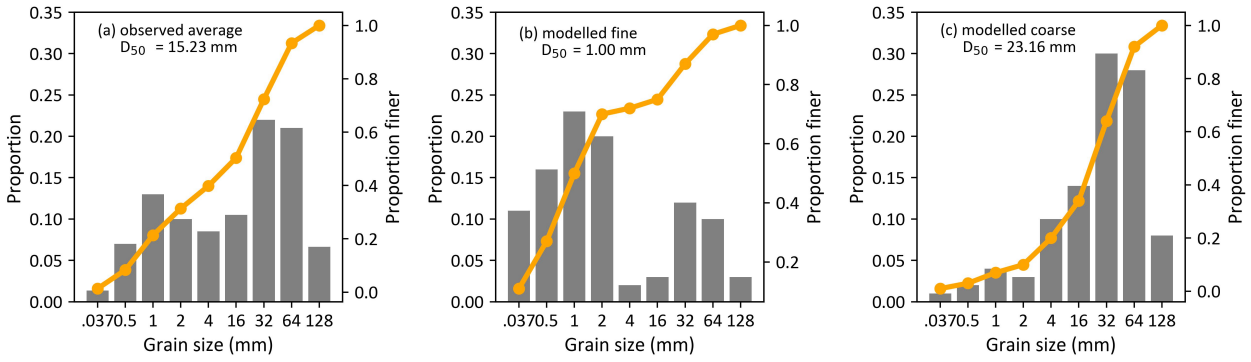

Figure 4: Sediment grain size distributions used in the numerical test cases: (a) scenario S1, average sediment GSD computed from field samples; (b) scenario S2, hypothetical fine sediment GSD; and (c) scenario S3, hypothetical coarse sediment GSD.

Figure 4 shows the sediment grain size distributions used in the numerical test cases listed in Table 1. To assess the sensitivity of model outputs to variations in grain size distribution, we altered the mean and standard deviation of the observed average distribution within prescribed uncertainty limits to create two additional grain size distributions that are also bimodal and have coarse and fine grain size proportions within the bounds of the observed distributions. Using this approach, similar to Wong et al. (2021) and Thapa et al. (2022), we produced the two additional plausible grain size distributions that we use in our model: a fine one and

a coarse one (Figure 4b and c, respectively). Tables 1 and 2 summarise the key sediment, vegetation and hydraulic parameters used in the model. A detailed parameter file is provided in the supplementary document S2. In Table 1, scenario S1 represents the observed average grain size distribution, whereas scenarios S2 and S3 are selected fine and coarse distributions, as shown in Figure 4.

2.3 Model spin-up

LEMs require a spin-up period for the results to become dynamically stable. For example, CAESAR-Lisflood may produce extremely high sediment transport rates during the early stage of a simulation as a result of initial surface roughness smoothing in the DEM and the fact that sediment grain size distribution is uniform across the catchment. Here, we assume that the bedrock is located far from the limit of maximum erosion, and so does not constrain sediment erosion. Following previous studies (Coulthard et al., 2013; Meadows, 2014; Coulthard and Van De Wiel, 2013; Ramirez et al., 2020; Feeney et al., 2020), we created a list of potentially sensitive parameters and available sediment transport formulas for the Nakkhu River, and opted to test the C-L model for different Manning roughness coefficients, lateral erosion parameters, and sediment transport formula selection. The C-L model was run for a 20-year spin-up period using a 10 m resolution DEM, a daily inflow hydrograph from 2001 (corresponding to an annual return period flood), and mean sediment grain size distribution data obtained from sieve analysis. Due to the lack of available sediment flux data at Tikabhairav, for all modelled scenarios presented in this study (parameters shown in Figure 5 and 8), sediment re-circulation was enabled (Coulthard et al., 2013). We analysed riverbed profiles (obtained using the channel extraction tool from LSDTopoTools [6]), outflow hydrographs, and annual sediment yields from the spin-up results to select appropriate model parameters for the study area.

Sediment fluxes were computed and compared for all three sediment transport approaches available in the C-L model. The average annual sediment yield of 1252 tonnes km^{-2} yr^{-1} was computed for the Bagmati basin from observed suspended sediment samples from 2011 to 2015 at Khokana, assuming bed load as approximately 35% of total sediment load, in agreement with previous observations in Himalayan rivers (Pratt-Sitaula et al., 2007; Turowski et al., 2010). We estimated sediment yields from the Nakkhu catchment using sediment outfluxes obtained from the C-L model, which are 74188, 10308, and 1081 tonnes km^{-2} yr^{-1} for Meyer-Peter and Müller, Einstein, and Wilcock and Crowe formulae, respectively. We converted these estimated sediment yields into uniform sediment erosion rates, which are 28.5, 3.96, and 0.42 mm yr^{-1} corresponding to the Meyer-Peter and Müller, Einstein, and Wilcock and Crowe sediment transport formulae. Based on literature on the Himalayas, the mean erosion rates are reported to be 0.5 to 2.5 mm yr^{-1} (Lupker et al., 2012; Blöthe and Korup, 2013; Morin et al., 2018), which are close to the value of sediment yield obtained using the Wilcock and Crowe formula. We selected the Wilcock and Crowe formula also because the estimated sediment yield for this model run was of a similar order of magnitude to the observed data, whereas the other two formulae greatly overestimated the sediment outflux.

To select an appropriate Manning roughness coefficient, we computed and compared simulated downstream flow hydrographs and annual sediment yield for different roughness values. We ran C-L using Wilcock and Crowe's sediment transport formula for a range of Manning roughness coefficients, varying from 0.030 to 0.050 s $m^{-1/3}$ using 0.005 s $m^{-1/3}$ increments, in accordance with values tabulated by Chow (1959)[7]. There was little variation between the simulated downstream flow hydrographs. The average annual sediment yield over the 20 year spin-up was compared with observed data from Khokana (DHM, Nepal). The best fit was obtained for a Manning's coefficient value of 0.04 s $m^{-1/3}$ (the estimated 1689 tonnes km^{-2} yr^{-1}

[6] https://simon-m-mudd.github.io/software/LSDTopoTools/

[7] http://www.fsl.orst.edu/geowater/FX3/help/8_Hydraulic_Reference/Mannings_n_Tables.htm

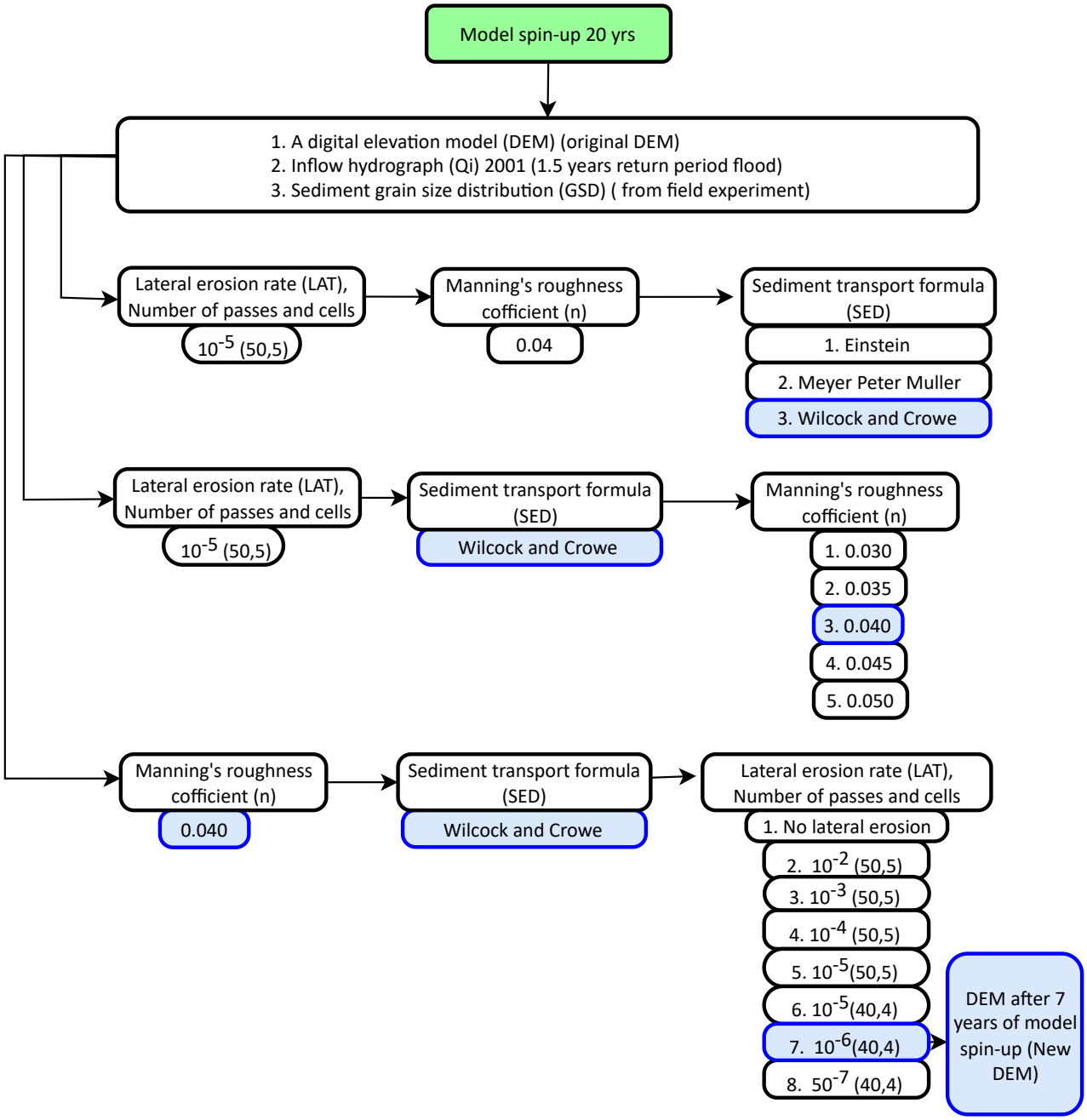

Figure 5: Flow chart highlighting key input parameters used for model spin-up. Blue-colored boxes indicate model parameters that were found to give the best fit to observables in the Nakkhu River.

was the closest case to the average observed). Therefore, the Manning roughness coefficient was set to 0.04 s $m^{-1/3}$ for all further simulations in this study.

Three parameters relate to the lateral erosion of the river require calibration: the lateral erosion coefficient, the number of passes for the edge smoothing filter, and the number of cells to shift erosion downstream, which is one tenth of the number of passes parameter according to model documentation[8]. A series of tests was therefore run to determine the best-fit for each of these parameters (Figure 5). We computed cumulative daily sediment throughput for 20 years (Figure 6) and compared post-spin-up river bed profiles against the original profile for all 8 cases (Figure 7). Modelled annual sediment yields from simulations for each grain size were normalised by the cumulative total sediment yield over 20 years and expressed as percentage yields consecutively, following Feeney et al. (2020). Across most scenarios, inter-

[8] https://sourceforge.net/p/caesar-lisflood/wiki/Home/

Table 1: Sediment parameters used; initial guidance obtained from model documentation. See also Meadows (2014), Feeney et al. (2020),Coulthard and Wiel (2006), Van De Wiel et al. (2007), Bates et al. (2010) and Coulthard et al. (2013). Parameters are unit-less unless stated otherwise.

Sediment grain size distribution	relative proportions		
Size (m)	observed average (S1)	modelled fine (S2)	modelled coarse (S3)
0.0000375	0.0135	0.04	0
0.0005	0.07	0.1	0.04
0.001	0.13	0.16	0.1
0.002	0.1	0.13	0.07
0.004	0.085	0.055	0.115
0.016	0.105	0.075	0.135
0.032	0.22	0.225	0.22
0.064	0.21	0.18	0.23
0.128	0.0665	0.035	0.09
Fall velocity (m s^{-1})	0.000129 (Van Rijn, 1989)		
Transport equation	Einstein, Meyer-Peter Müller, and Wilcock & Crowe (2003)		
Max velocity to calculate shear stress (m s^{-1})	5		
Max erode limit (m)	0.02		
Active layer thickness (m)	0.1		
Proportion of output sediment recirculated	1		
In-channel erosion rate	10		
Lateral erosion rate	0, 10^{-2}, 10^{-3}, 10^{-4}, 10^{-5}, 10^{-6}, 5×10^{-7}		
No. of passes for edge smoothing filter	40, 50		
No. of cells to shift erosion downstream	4, 5		
Max diff. for cross-channel smoothing	0.0001		

annual sediment yield variability stabilised after year 7, thus defining the spin-up duration (Figure 6).

Table 2: Vegetation and other parameters, initially obtained from model documentation. See also Meadows (2014), Feeney et al. (2020), Coulthard and Wiel (2006), Van De Wiel et al. (2007), Bates et al. (2010) and Coulthard et al. (2013). Parameters are unit-less unless stated otherwise.

Vegetation	
Vegetation critical shear strength (N m^{-2})	180
Grass maturity (years)	5
Proportion of erosion allowed at maturity	0.1
Slope failure threshold (degrees)	85 (maximum slope identified from DEM)
Flow model	
Input/output discharge difference allowed (m^3 s^{-1})	0.3
Min - max discharge for depth calculation (m^3 s^{-1})	0.1 - 100
Water depth to exceed before erosion (m)	0.01
Slope for edge cells (m m^{-1})	0.01
Evaporation rate (m day^{-1})	0.00000001
Courant number	0.4
Froude number (flow limit)	0.8
Manning's roughness value, n (s $m^{-1/3}$)	0.030, 0.035, 0.040, 0.045, 0.050

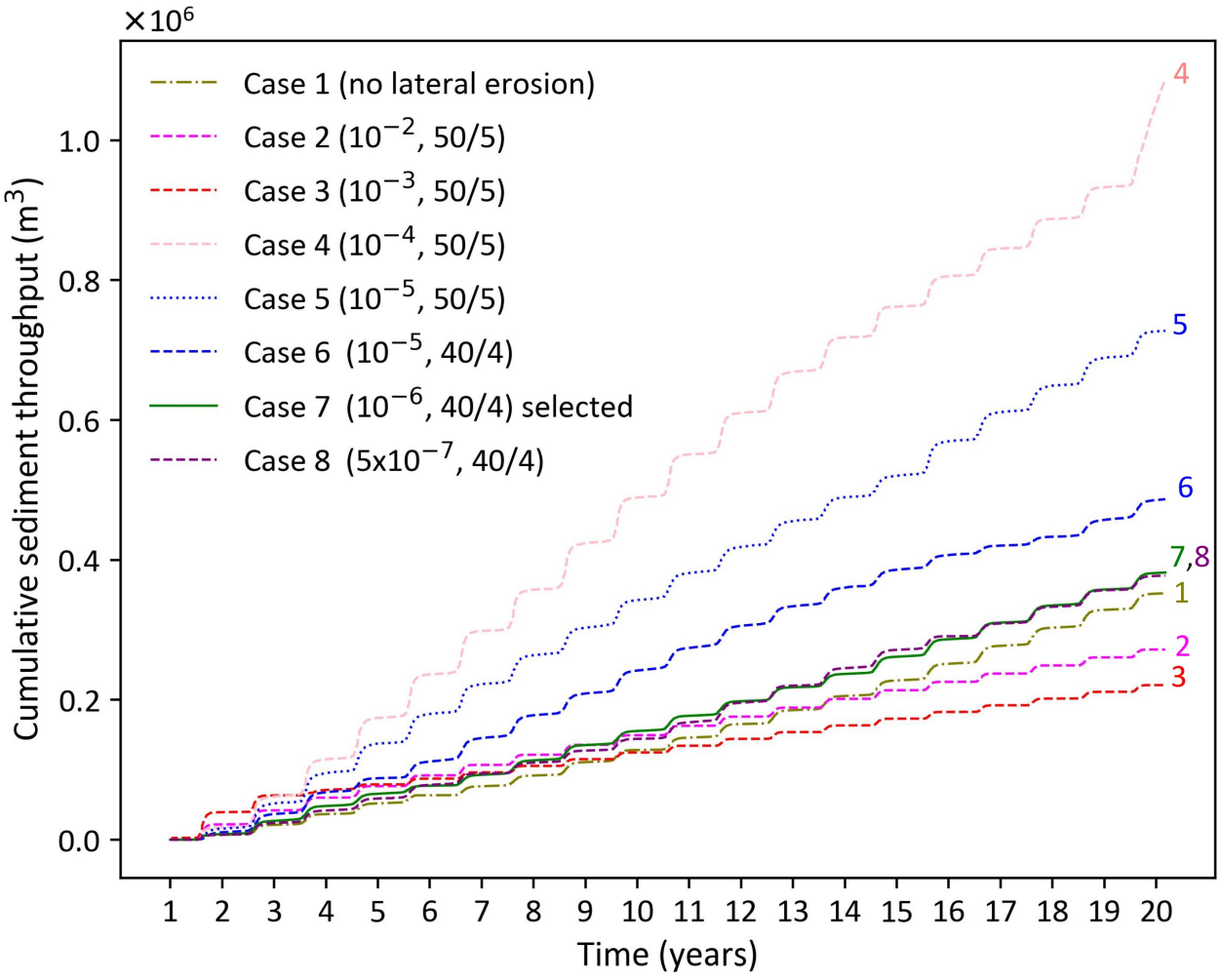

Figure 6: Cumulative sediment throughput over 20 years for different lateral erosion parameters. In the legend, the first value refers to the lateral erosion coefficient and the fraction refers to the number of passes of the edge smoothing filter / the number of cells used to shift lateral erosion downstream.

In the downstream part of the river profile, a high value of lateral erosion coefficient (e.g. case 3: 10^{-3}) caused increased bed scouring, whereas a low caused deposition (e.g. case 6: 10^{-5}) (Figure 7). Case 7, with a lateral erosion coefficient of 10^{-6}, 40 passes of the edge smoothing filter and 4 cells to shift lateral erosion downstream resulted in a post-spin-up river profile most similar to the original river profile (Figure 7), and the parameters used in this case were selected for all further scenarios presented herein.

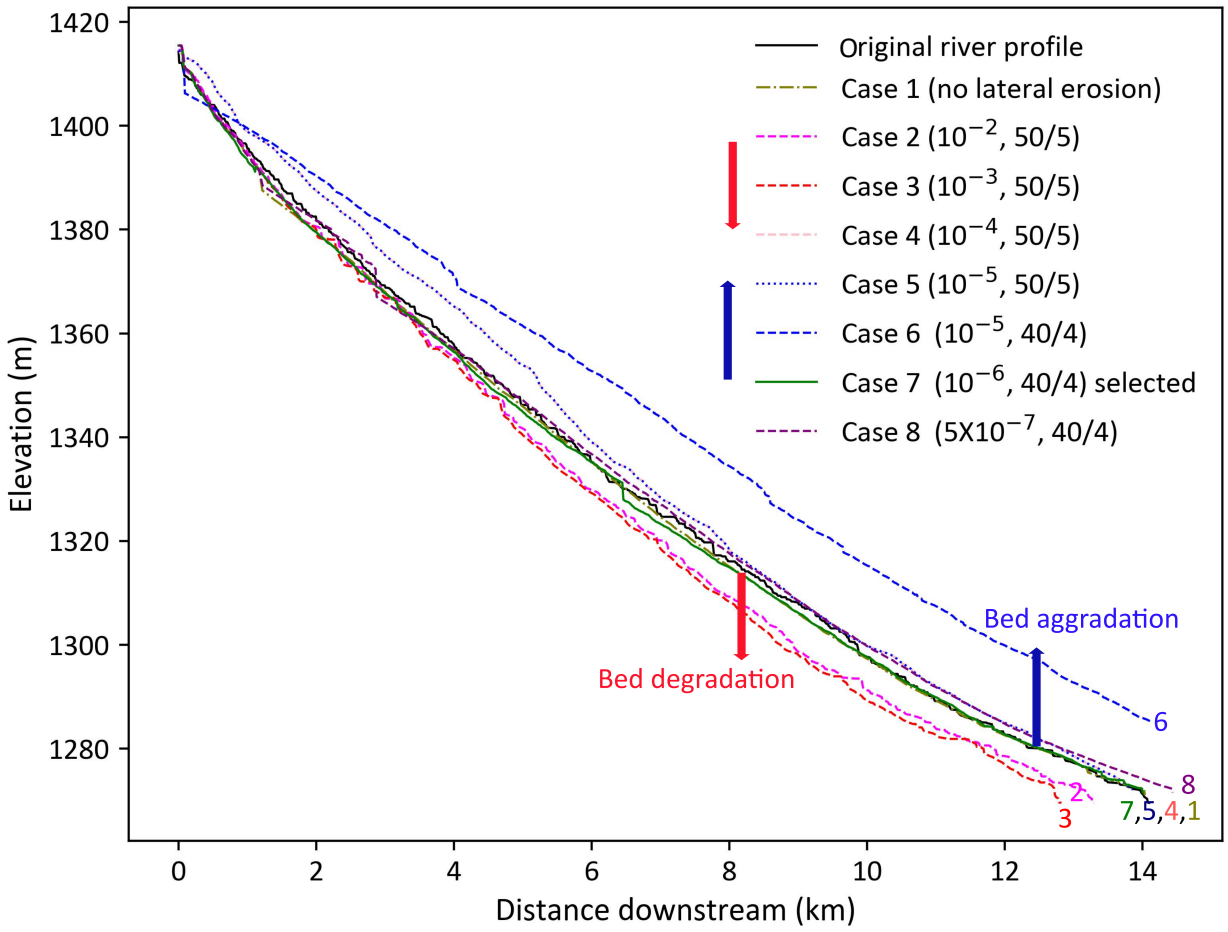

Figure 7: Original river bed profile and riverbed profiles obtained after model spin-up using different lateral erosion parameters. In the legend, the first value refers to the lateral erosion coefficient and the fraction refers to the number of passes of the edge smoothing filter / the number of cells used to shift lateral erosion downstream.

In summary, the spin-up tests demonstrated that the best DEM in a "dynamic equilibrium" (i.e., with output stabilised) for the annual return period flood of 2001 was obtained using the Wilcock and Crowe sediment transport formulae, a lateral erosion coefficient of 10^{-6}, 40 passes for the edge smoothing filter, 4 cells to shift lateral erosion downstream, and a Manning roughness coefficient of 0.04 s $m^{-1/3}$ after a 7-year spin-up duration (Figure 5).

In the following model simulations, the post-spin-up DEM was used as the initial terrain. The flowchart in Figure 8 indicates the parameters utilised in the sensitivity analysis to explore the impact of sediment grain size distribution on flooding and morphological change. All GSD tests used the same DEM for the initial bed conditions. The impact of sediment transport on flooding was evaluated by computing water depths and area of inundation for simulations with and without sediment transport and for different sediment GSDs. The effect of discharge magnitude and sediment GSD on changes to the river morphology was investigated by calculating the daily difference in erosion/deposition volume from the integrated spatial change in DEM and the cumulative volume change over each year. The geometry of the river cross sections and

the lateral migration of the channel were also examined.

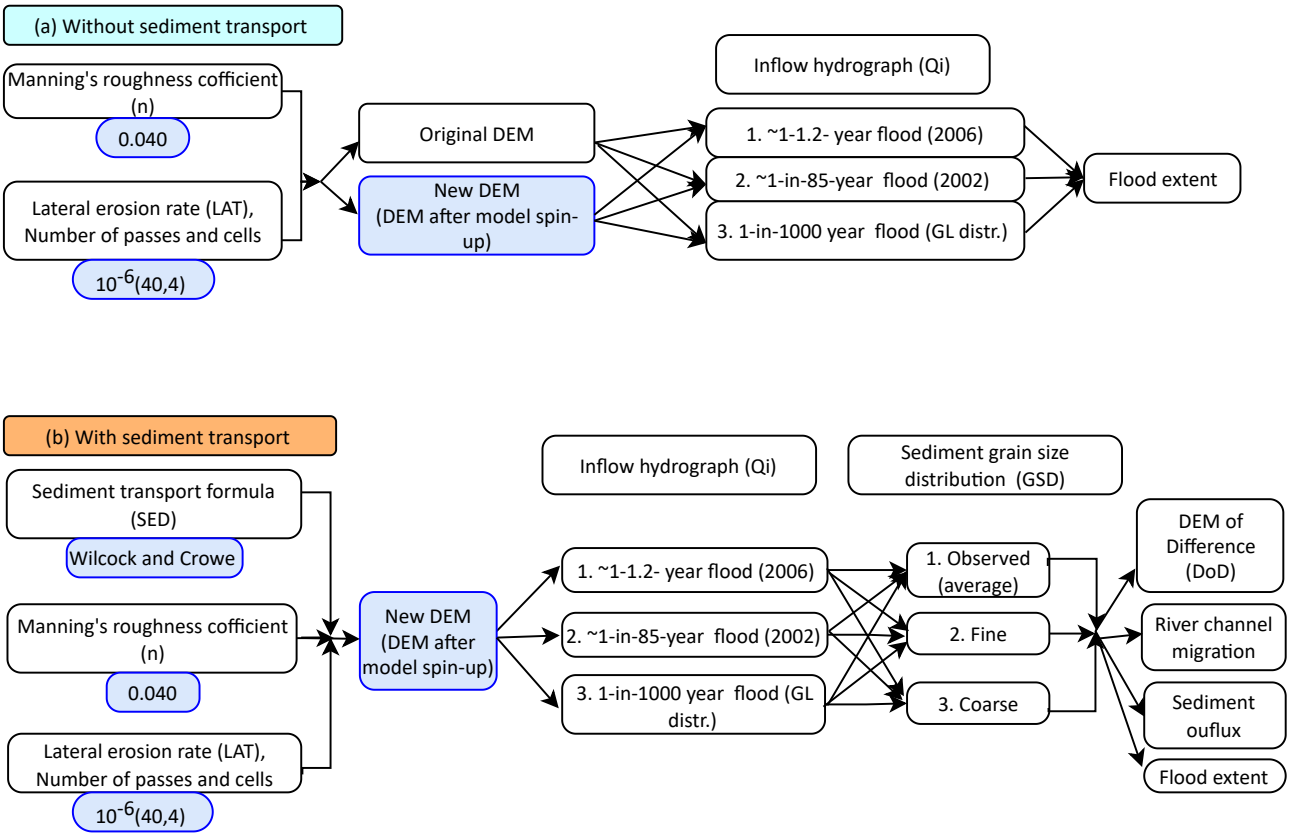

Figure 8: Flow chart highlighting key input parameters used for sensitivity analysis: (a) without, and (b) with sediment transport. Blue-colored boxes indicate model parameters that were found to give the best fit to observations of the Nakkhu River.

3 Results

A total of 29 simulations were carried out for the Nakkhu River, including 14 initial runs to calibrate the sediment transport formulae, Manning's roughness coefficient, and lateral erosion parameters described above. This section examines simulations of three flood magnitudes corresponding to 1.2-year (2006), 85-year (2002), and 1000-year return periods (predicted), combined with three GSDs (average, fine, coarse), and no-sediment cases, to evaluate: 1) sediment transport under different flood magnitudes, and 2) the impact of sediment transport and discharge magnitude on river morphology and inundation. For the no-sediment cases, we ran models using the original DEM and the post-spin up DEM.

3.1 Sediment transport and river discharge

Total daily sediment transport exhibited a linearly positive correlation with daily water discharge regardless of flood return period and sediment GSD, with a Pearson correlation coefficient, R, ranging from 0.78 to 0.97. Specifically, R is 0.82, 0.93, and 0.80 for average, fine, and coarse GSD for the 1-in-1.2 year flood (2006), rising to 0.97, 0.94, and 0.95 for the 1-in-85 year flood (2002) and 0.96, 0.94, and 0.95 for the 1-in-1000 year flood (Figures 9, 10 and 11). This implies that sediment transport exhibits a strong linear correlation with river discharge for extreme floods of 85- and 1000-year return periods and a less strong correlation for the low flood with a 1.2 year return period. Furthermore, the correlation is strongest for the 1.2-year return period flood when the fine GSD is used (Figure 9d), and strongest for the high floods (85-year and 1000-year) in the observed average and coarse GSD cases (Figure 10b and f and 10b and f).

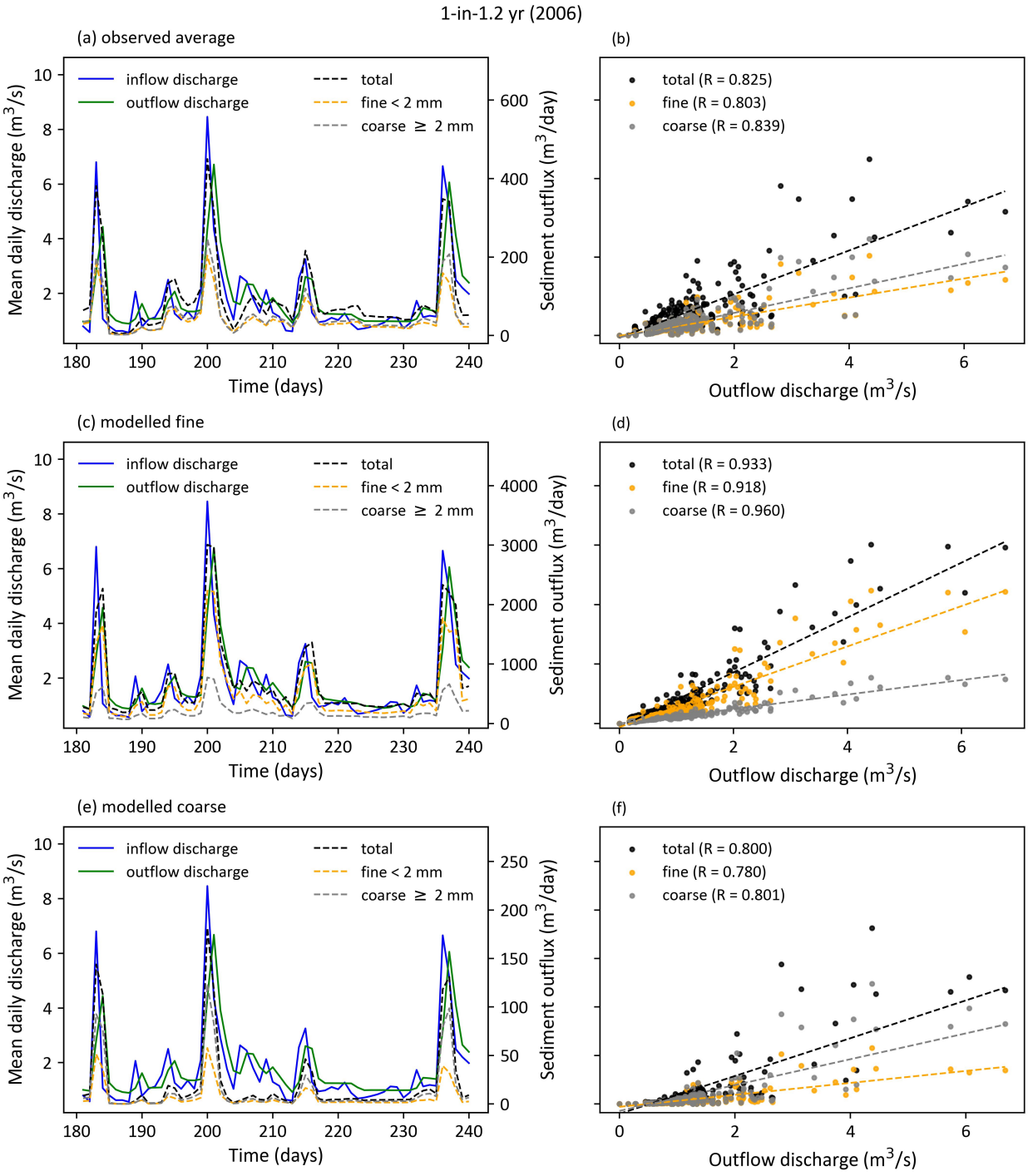

Figure 9: Computed water-sediment flows in the Nakkhu River. Left hand panels show inflow and outflow discharge hydrographs and daily sediment throughput time series for the Nakkhu River in 2006 (i.e., 1.2-year return period flood) for (a) observed GSD, (c) fine GSD, and (e) coarse GSD. Right hand panels (b, d and f) show corresponding variations in sediment throughput with outflow river discharge for the three GSDs. The results display total, finer ($D < 2$ mm), and coarser ($D \geq 2$ mm) sediment throughputs obtained in pre-monsoon to post-monsoon periods during which the most significant changes were observed.

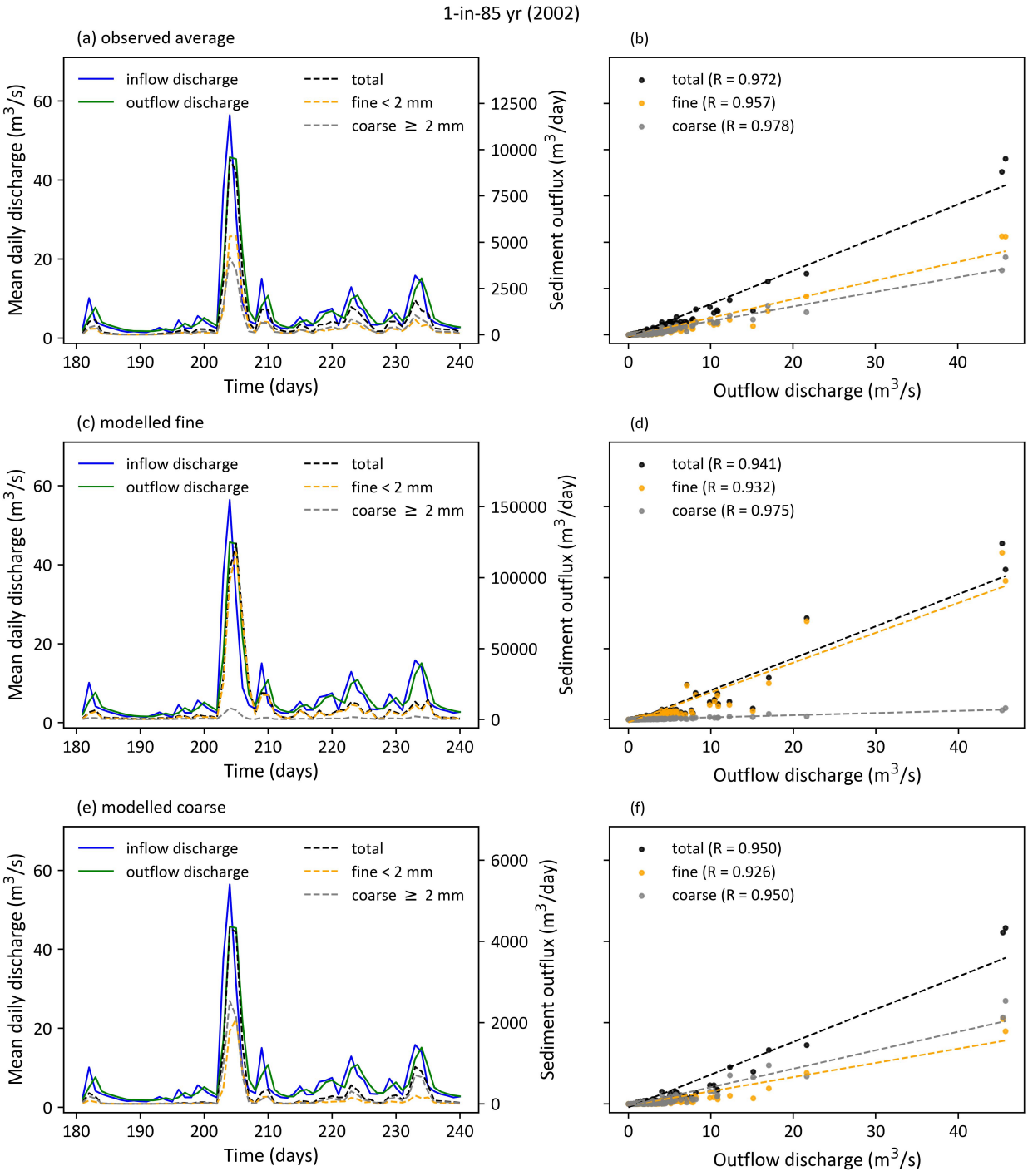

Figure 10: Computed water-sediment flows in the Nakkhu River. Left hand panels show inflow and outflow discharge hydrographs and daily sediment throughput time series for the Nakkhu River in 2002 (i.e., 85-year return period flood) for (a) observed GSD, (c) fine GSD, and (e) coarse GSD. Right hand panels (b, d and f) show corresponding variations in sediment throughput with outflow river discharge for the three GSDs. The results display total, finer ($D < 2$ mm), and coarser ($D \geq 2$ mm) sediment throughputs obtained in pre-monsoon to post-monsoon periods during which the most significant changes were observed.

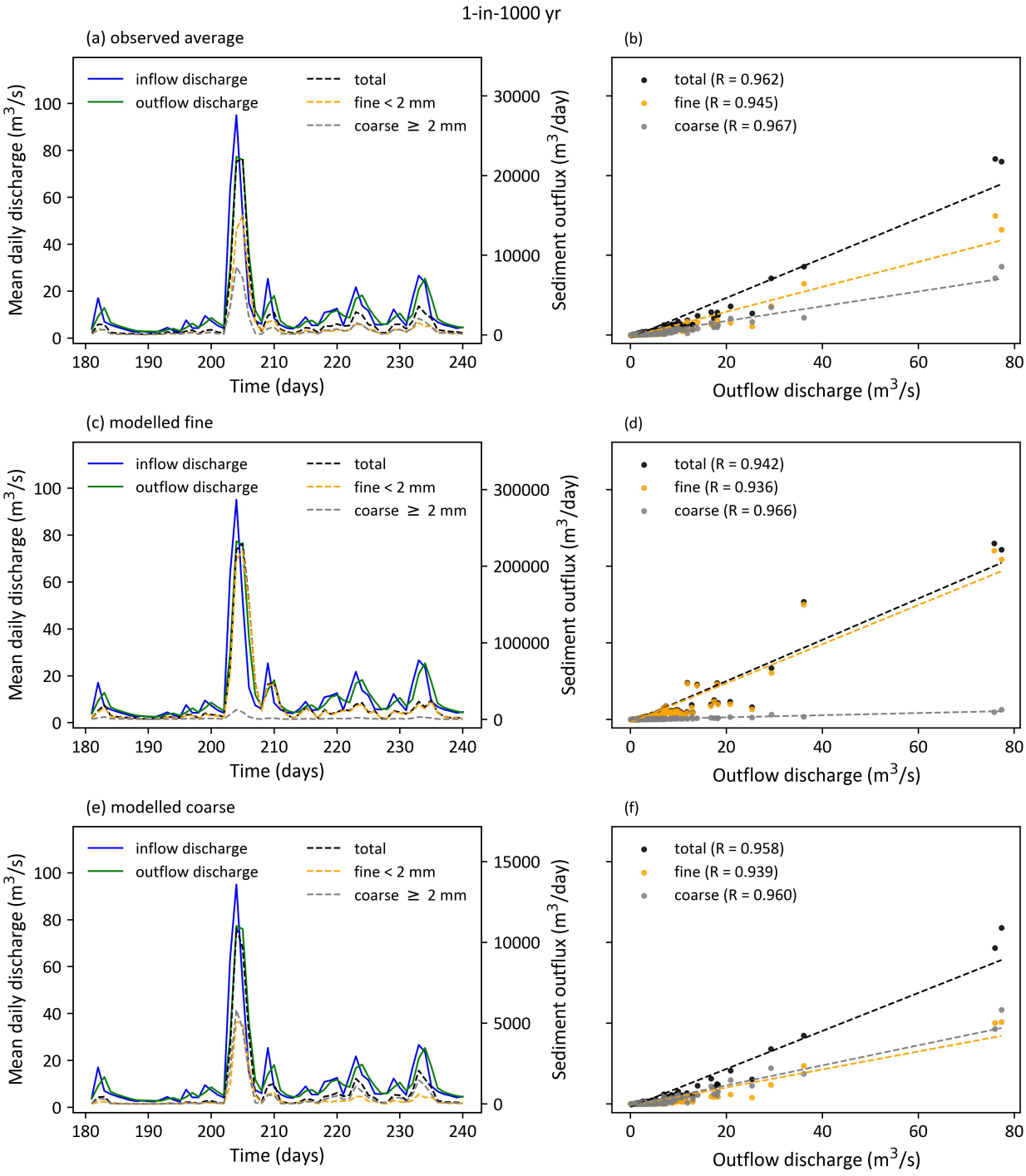

Figure 11: Computed water-sediment flows in the Nakkhu River. Left hand panels show inflow and outflow discharge hydrographs and daily sediment throughput time series for the Nakkhu River experiencing 1000-year return period flood for (a) observed GSD, (c) fine GSD, and (e) coarse GSD. Right hand panels (b, d and f) show corresponding variations in sediment throughput with outflow river discharge for the three GSDs. The results display total, finer ($D < 2$ mm), and coarser ($D \geq 2$ mm) sediment throughputs obtained in pre-monsoon to post-monsoon periods during which the most significant changes were observed.

3.2 Effect of sediment on morphology

To investigate the influence of grain size distribution on river bed morphology, we subtracted the initial DEM from the final DEM after one year of model simulation for each scenario. This allowed us to analyse changes to river cross-sections, and estimate total deposition and erosion volumes by integrating all positive and negative values, respectively. For all coarse GSD cases, regardless of peak flood magnitude, the overall sediment volume budget obtained by subtracting the total erosion volume from the total deposition volume was almost zero, indicating that deposition and erosion processes remained in balance. However, the volume budget for the 1.2-year return period flood was slightly out of equilibrium by maxima of 6% and 0.5% for the fine and average GSD cases. It should be noted that the imbalance in sediment volume budget may be influenced by the long time scale required for suspended sediment to settle fully within the model domain, explaining the higher value for fine GSD. Because sediment erosion and deposition are approximately in balance, we use the deposition volume as a proxy for sediment transport intensity and corresponding morphology. Figure 12 shows that the deposited sediment volume obtained for the fine GSD is larger than that for the average and coarse GSDs at all flood magnitudes. For the 1.2-year return period flood, the total deposited volume predicted for the fine GSD is ∼3 and 5.5 times that obtained for the average and coarse GSDs. These multipliers reduce to ∼1.1 to 1.3 for the 85-year return period flood and the 1000-year return period flood. For the fine GSD, the total deposition volume obtained for 85-year flood is about double that of 1.2-year flood (Figure 12).

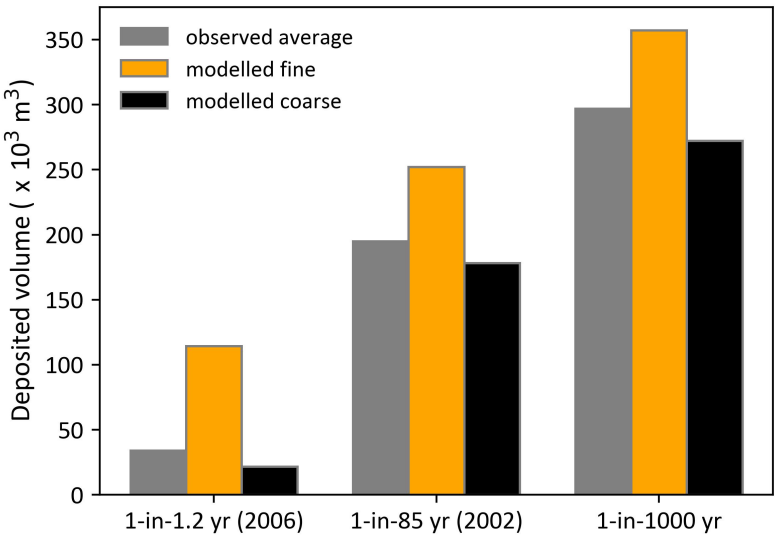

Figure 12: Deposited sediment volume obtained from DEM of Difference between pre-flood and post flood bed morphologies of the Nakkhu River reach for observed average, fine and coarse grain size distributions and 1.2-year return period flood [left], 85-year return period flood [middle] and 1000-year return period flood [right].

The box and whisker plots in Figure 13 present a statistical summary of erosion and deposition depth distributions obtained for all nine sediment transport simulations. The mean erosion depth is invariably larger than the mean deposition depth in all cases. This implies that bed erosion is more localised than deposition in the Nakkhu River after a flood event. Figure 14 displays the cumulative daily deposited volume and river discharge time series over one year for different grain size distributions and flood magnitudes. In the extreme flood cases, there is a step increase in deposited volume as the peak of the flood wave passes. Computation of total and fractional sediment yields reveals that the bimodal sediment mixture with finer GSD leads to sediment transport rates that are significantly higher throughout the year than with either average or coarser GSD (for all simulated hydrographs).

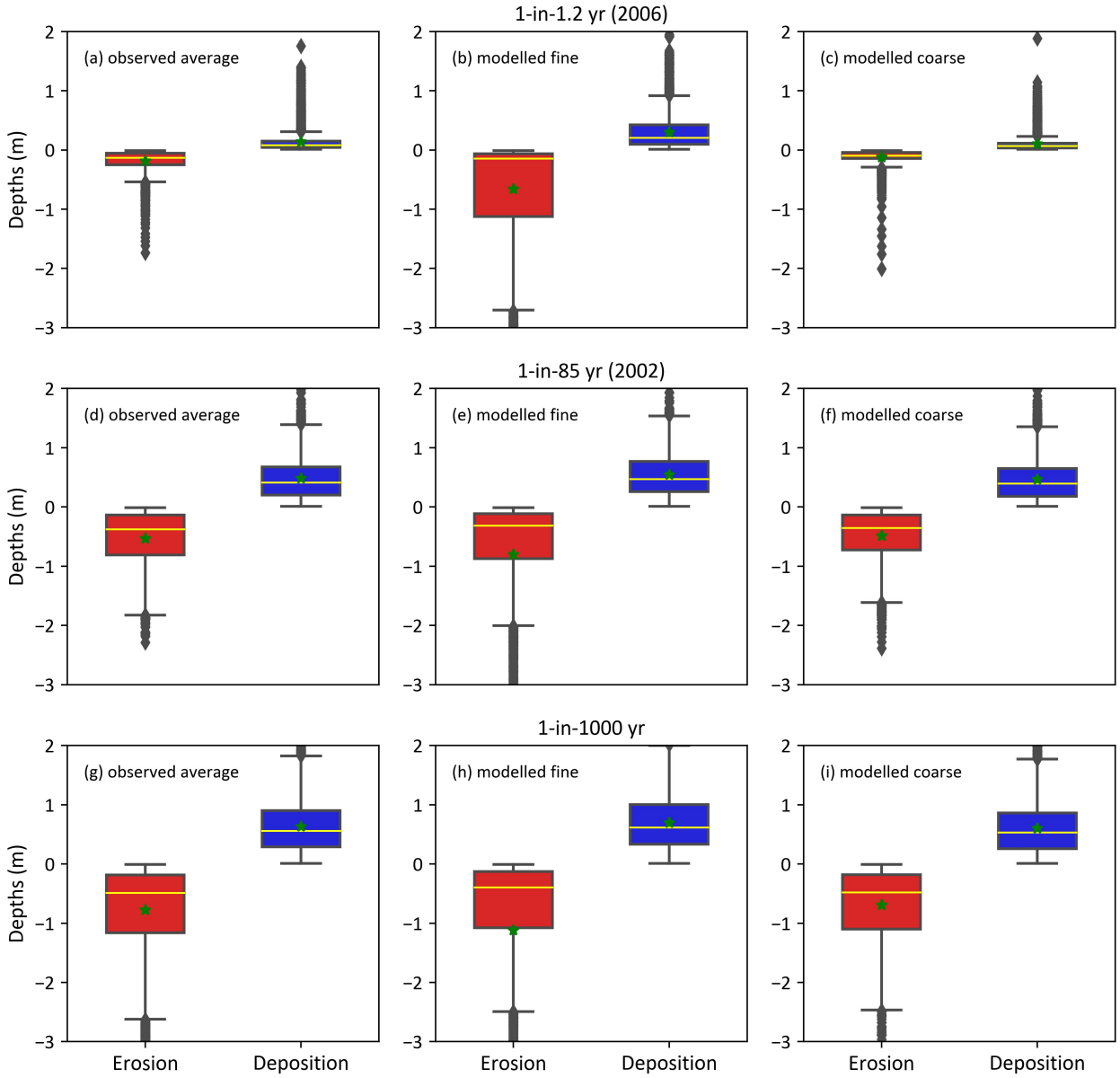

Figure 13: Box and whisker plots of the distribution of erosion (red) and deposition (blue) depths in the Nakkhu River reach obtained for observed average GSD (left column), modelled fine GSD (middle column), and modelled coarse GSD (right column), and flood return periods of 1.2 years (top row), 85 years (middle row), and 1000 years (bottom row).

Figure 15a indicates notable locations that exhibited channel plan-form and/or elevation changes, including changes to the original river thalweg. Other subplots of Figure 15 present: (b) the lateral channel migration; (c-e) DEMs of difference; and (f-i) flood extent maps near downstream location XS18. Figure 16 presents cross-section profiles at the downstream location, XS18, before and after 1.2-, 85-, and 1000-year return period events (rows) for the three different GSDs (columns). At XS18, field observations of the maximum deposition and erosion depths were recorded as 1.2 m and 1 m, respectively, after the 2021 flood, which had a discharge similar to the 1.2-year return period flood. This magnitude of deposition is similar to the maximum simulated deposition for the fine GSD scenario under the 1.2-year discharge. However the simulated erosion at this location is underestimated (Figure 16b). In the present simulation of the 1.2-year flood, at XS18 the fine GSD scenario predicts greater morphological change compared to the average and coarse GSD. For the 1-in-85 year and 1-in-1000 year scenarios a similar magnitude of erosion and deposition is observed across all GSDs.

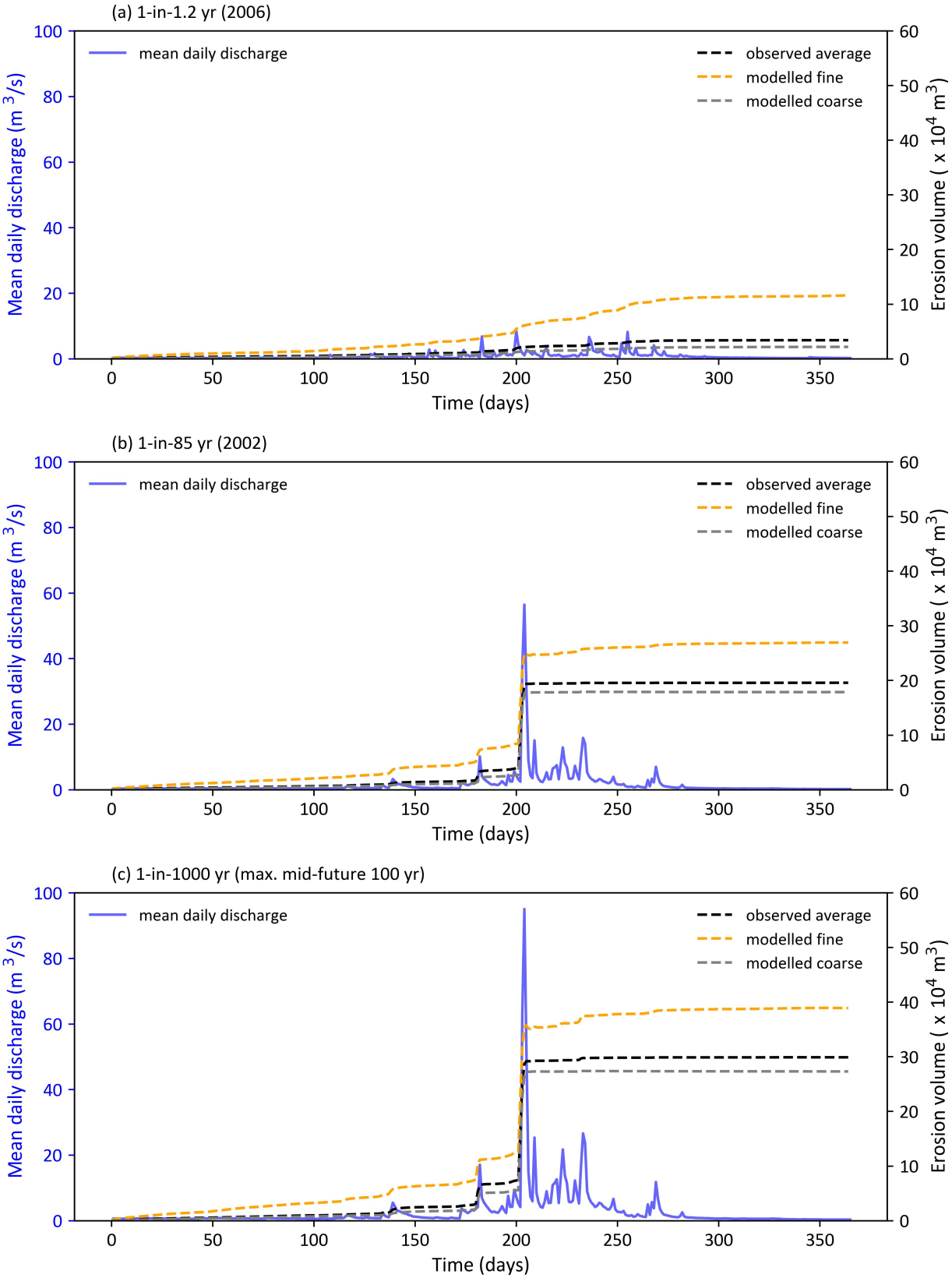

Figure 14: Time histories of cumulative daily volume of sediment deposition with superimposed discharge hydrograph for the Nakkhu River, obtained for fine, average, and coarse grain size distributions: (a) 85-year return period flood of 2002; (b) 1.2-year return period flood of 2006; and (c) 1000-year return period flood.

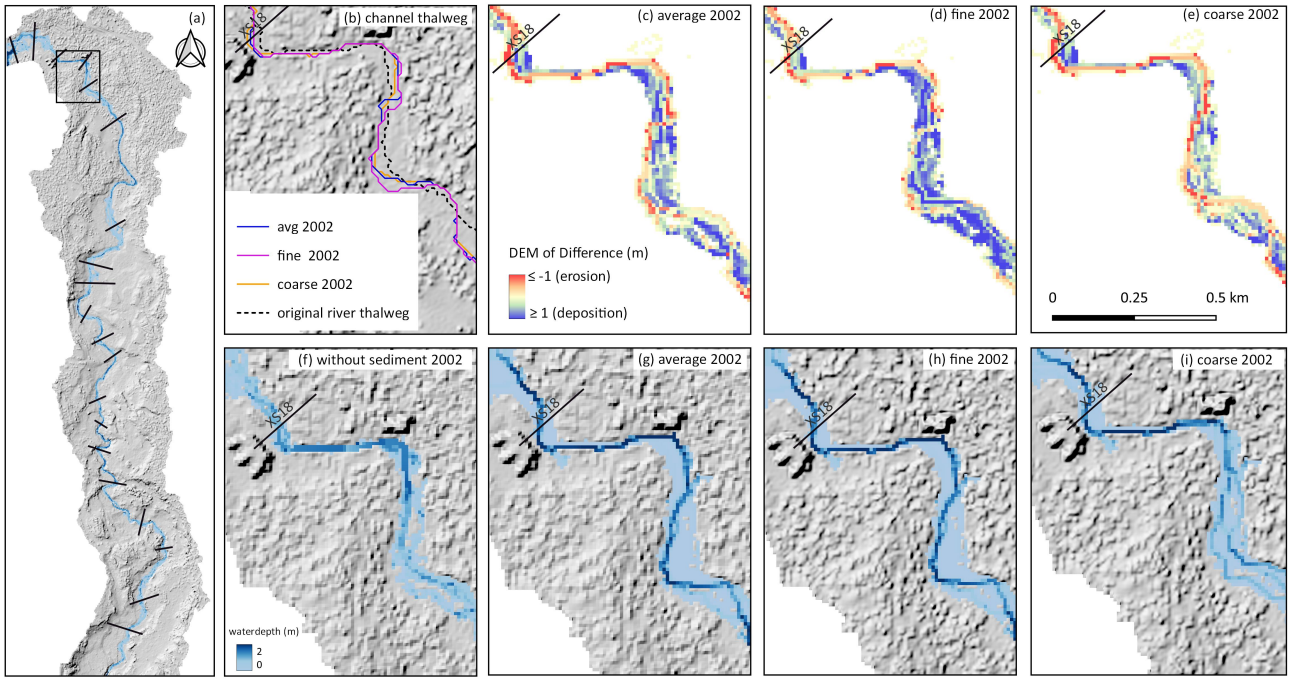

Figure 15: Morphological change along the Nakkhu River: (a) morphology change locations; (b) lateral channel migration; (c-e) erosion and deposition maps from DEM of difference, (f-i) flood extent maps in the downstream region near Location 18.

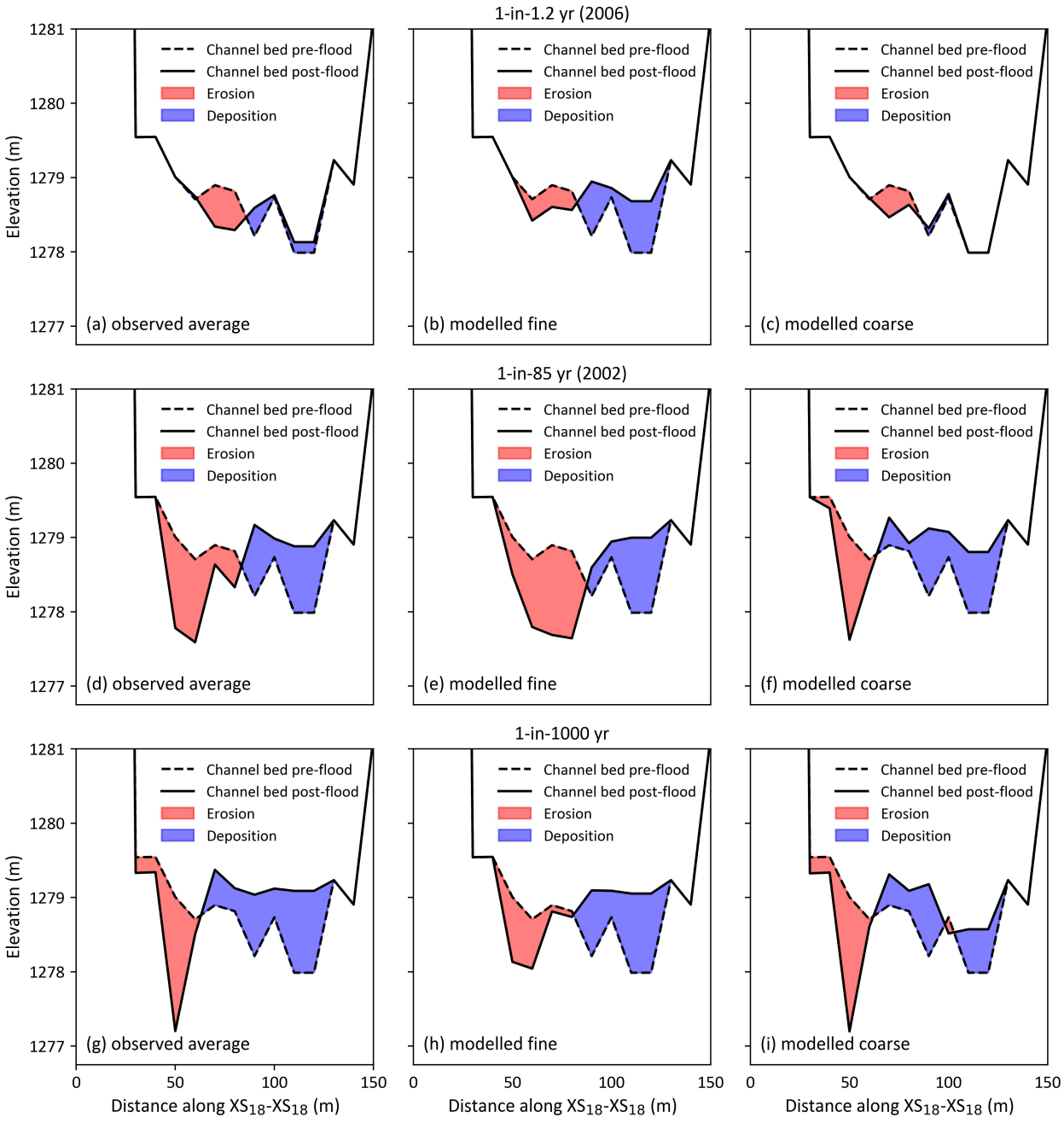

Figure 16: River cross-section profiles at Location 18 (shown in Figure 15) for average GSD (left column), fine GSD (middle column), and coarse GSD (right column) subject to 1.2-year (upper row), 85-year (middle row), and 1000-year (lower row) return period flood events.

3.3 Effect of sediment on inundation

The relative impact of grain size distribution on flood inundation is greater for the high-frequency, low-intensity 1.2-year return period flood than the low-frequency 85-year and 1000-year return period flood events (Figure 17). For the 1.2-year return period flood, the computed inundation areas obtained for the observed average GSD, fine GSD, coarse GSD and no sediment are 0.26, 0.32, 0.24 and 0.20 km^2, respectively. This implies that increased morphological change observed in the finer the grain size scenarios (Figure 15) leads to increased flood inundation extent. Although these values seem low compared to large Himalayan rivers, the area of the Nakkhu River in the study reach is only 0.2 km^2. By classifying the inundation area according to flow depth, we can see that the inundation area with water depth below 0.5 m is larger when sediment transport occurs than for no sediment, whereas the inundation area for water depth exceeding 0.5 m is greater for no sediment regardless of flood return period. We believe this result is due to the infilling of local depressions and erosion of local peaks in the DEM river and floodplain. As such, sedimentation "smooths" the DEM locally and causes shallower inundation in some regions. The model is more sensitive to choice of sediment grain size distribution for more frequent, lower-intensity floods. The estimated flood inundation area for a 1.2-year return period flood with sediment transport is 21%, 50%, and 13% higher for the observed average, fine, and coarse GSD cases than the no sediment transport case. However, the relative differences converge for the extreme return period floods; where the inundation is 13%, 15%, and 14% higher than the no sediment case for the average, fine, and coarse GSDs in the 85-year return period flood, and about 9% higher for all GSD cases in the 1000-year return period flood.

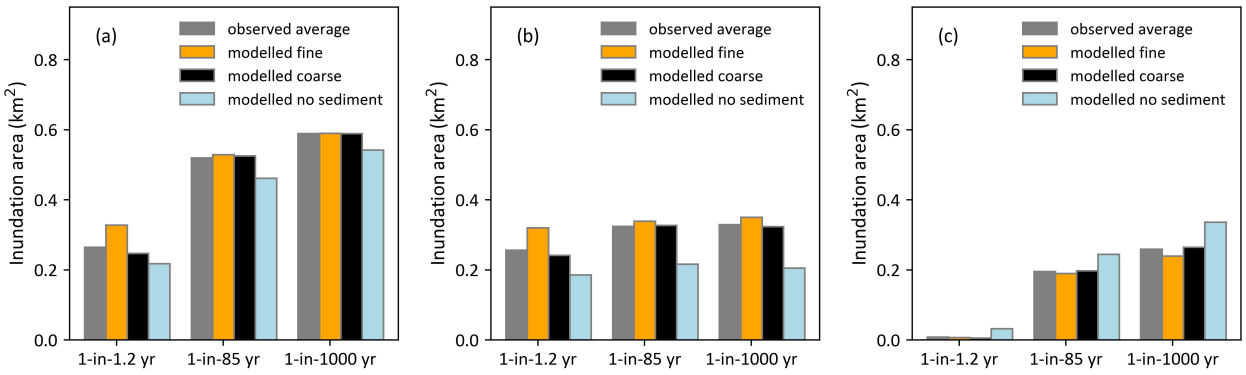

Figure 17: Histogram showing inundation areas after subtracting river channel obtained for 1.2-, 85-, and 1000-year return period floods: (a) within the entire model domain regardless of water depth; (b) water depth ≤ 0.5 m; and (c) water depth > 0.5 m.

4 Discussion

This paper has shown how the morphology of the Nakkhu River is affected for different sediment grain size distributions and flood magnitudes (ranging from annual to extreme flood events, the latter incorporating the effect of climate change). The response of the river morphology to sediment flux has a direct knock-on effect on flood inundation and potential flood risk to life and property. In the Nakkhu River, annual sediment erosion/deposition volume(s) and changes to river geometry are sensitive to the grain size distribution of the sediment supplied to the river. It is common practice worldwide, with Nepal no exception, to neglect sediment transport in flood hazard assessment; our study highlights the importance of accounting for sediment transport and sediment grain size distribution when estimating inundation. In general, the

effect of bed aggradation tends to be overlooked in flood risk mapping exercises because of the extra time and resources required for river bed surveys and updating the DEM with historical data. This, in turn, leads to an underestimation of total flood inundation and associated flood risk. We have found a clear signal that inundation increases when we include sediment transport in the flood models, highlighting the need to include sediment in future flood studies.

The scenario tests showed that sediment transport increases monotonically with magnitude of flood discharge. This correlation proved to be strongest for the fine GSD in low flows and for the average and coarse GSDs in the extreme flood flows (> 85-year return period). This suggests that coarse sediment beds are more stable than fine beds in the Nakkhu River because they can only be mobilised during low-frequency high-intensity flood events.This supports the conclusion of previous research by Sambrook Smith and Nicholas (2005), who state that even moderate additions of fine sediment can smooth the bed sufficiently to reduce shear stress and that sand dominates the bed downstream. The parametric dependencies established in the study have clear implications for an improved understanding of fractional inter-granular effects at the bed surface and their influence on graded sediment transport processes within natural fluvial channels under flood flow hydrographs. It is obviously important to understand this phenomenon where activities such as mining selectively extract certain types of bedload material. For example, in the Nakkhu River, the major sources of sediment are fine waste material from upstream gravel mining and coarse sediment from natural landslides. Future changes to the mining activity or increased landslide activity upstream could modify the grain size distribution in the river and subsequent morphology and inundation during the monsoon season. In addition, we found that sediment transport and morphological change were more intense during the rapid rising limb of the hydrograph, but more subdued during the receding limb, regardless of flood magnitude, supporting previous research such as by Miller and Friedman (2009). Understanding these sediment transport patterns could help to improve sediment management and regulate future mining activity.

Our work confirms the importance of sediment grain size distribution and associated bed aggradation on flood inundation of a river in the Himalayas. During highly frequent floods (1.2-year return period), sediment transport for a fine GSD had a much greater effect on bed erosion and deposition compared to the average and coarse GSD cases, suggesting that these low-magnitude floods are dominated by fine sediment transport. Sediment deposition in the downstream reach reduced the water carrying capacity of the channel and caused more inundation; this phenomenon was most pronounced for the fine GSD case. In high-intensity, low-frequency floods (85-year and 1000-year return periods), morphological change and inundation were similar regardless of GSD. This was most pronounced for the 1000-year flood where all GSD cases resulted in the same inundation area. This suggests that when estimating flood inundation for high-frequency, low-intensity flood events, accurate grain size measurements are required. However, for high-intensity, extreme flood assessment, an approximate grain size distribution is adequate because most sand and gravel particles will be mobilised during an extreme event. This is an important finding for modelling flood hazards in which sediment transport is significant. Our findings demonstrate that the influence of sediment transport is largest in finer grained systems responding to frequent flooding. By contrast, coarser grained systems require higher magnitude events to impact on channel morphology and hence the sediment distribution. The implication is that in modelling frequent floods the approximation to the grain size distribution is important; however for higher magnitude floods where there is equal mobility of grain sizes, parameterisation of grain size distributions is less important.

To date, hydrologists in Nepal have not had the resources to conduct long-term data collection on water and sediment carried by its rivers. This means that the traditional use of extreme value statistical distributions to model the frequency of occurrence of flood events is highly limited. Moreover, ongoing and future land use and climate changes render the use of such extreme value distributions debatable, with climate change for example greatly increasing

the likelihood of extreme floods. Although we fitted three different extreme value distributions to annual peak flow discharge data from the Nakkhu River, the overall duration (26 years) of the observed data is insufficient to give a reliable means of forecasting the likelihood of long-term future flood events (Hirabayashi et al., 2013) (even without accounting for climate change and human interference). Of the three distributions considered, the generalized logistic distribution gave a better fit to the 26 years observed data at Khokana hydrological station. We note that the 1000-year flood modelled here is approximately equal to the maximum mid future 100-year return period flood due to climate change according to the Shrestha et al. (2023)'s general circulation model projections. As outlined by Shrestha et al. (2023), the range of possible future conditions is large, but we have chosen to use the mid-range of output values from the forecasts.

There is uncertainty in the model resulting from the multiple parameters some of which need calibration for each setting. One includes the refinement of the DEM, which at 10 m resolution is many scales larger than the sediment particles, ripples, and dunes. At higher refinements, more topographic features come into view which could allow more accurate modelling of sediment features such as gravel bar migration. In addition, the model requires a selection of empirical and tuning parameters such as lateral erosion parameters and Manning coefficient. In order to carry out a more thorough sensitivity analysis of the C-L model and parameters, more detailed data such as longer time series of sediment flux, discharge, and topographic surveys pre and post major floods would be required. Despite the limited data, through our sensitivity analysis and variation in water discharge and grain size combinations, we have shown the importance of accounting for sediment transport in flood analysis, and a need for more long-term monitoring of sediment and river morphology.

5 Conclusions

This paper presents the first model that explores the impact of sediment grain size and future climate change on bed morphology and flood inundation in a Himalayan River. Detailed analysis of the role of sediment on flood risk is critical in sediment-rich mountain catchments, particularly where urban development impacts land-use change incorporating industries such as sand mining. To achieve this, we use the CAESAR-Lisflood landscape evolution model applied to a 10 m DEM dataset of the Nakkhu River in the Kathmandu Valley. The principal results show that inclusion of sediment transport in numerical models leads to modifications of river channel morphology and results in increased flood inundation over the floodplain for modelled small and large flood events. In addition, sediment flux through the model river increases approximately linearly with discharge, particularly for high flow events. Similarly, grain size distribution affects inundation extent, with the effect most pronounced for annually recurring events that predominantly transport fine sediment rather than coarse sediment. During less frequent (higher magnitude) flood discharge, all grain sizes are mobilised and the impact of grain size distribution on river morphology and inundation is diminished. This broadly implies that fine-grained sediment-rich rivers are most sensitive to changes in flood inundation. The CAESAR-Lisflood model has enabled exploration of the role of sediment calibre, which is shown to be highly sensitive to the coefficient that captures the lateral erosion of the channel banks, highlighting the importance of calibration.

References

M. Attal. Linkage Between Sediment Transport and Supply in Mountain Rivers 12 . 2 Sediment Supply to Mountain Rivers and its Influence on the Characteristics of the Sediment Available for Fluvial Transport. *Gravel-Bed Rivers: Processes and Disasters*, 2017.

M. Attal and J. Lavé. Changes of bedload characteristics along the Marsyandi River (central Nepal): Implications for understanding hillslope sediment supply, sediment load evolution along fluvial networks, and denudation in active orogenic belts. *Special Paper of the Geological Society of America*, 398(09):143–171, 2006. ISSN 00721077. doi: 10.1130/2006.2398(09).

D. B. Basnyat, D. Shrestha, S. Thapa, S. Bajimaya, M. Maharjan, S. Shrestha, S. Dhungana, et al. Post-flood assessment of the 2019 flooding in the bagmati river basin, nepal. *Journal of Development Innovations*, 4(1):20–47, 2020.

P. D. Bates and A. De Roo. A simple raster-based model for flood inundation simulation. *Journal of hydrology*, 236(1-2):54–77, 2000.

P. D. Bates, M. S. Horritt, and T. J. Fewtrell. A simple inertial formulation of the shallow water equations for efficient two-dimensional flood inundation modelling. *Journal of Hydrology*, 387 (1-2):33–45, 2010. ISSN 00221694. doi: 10.1016/j.jhydrol.2010.03.027. URL http://dx.doi.org/10.1016/j.jhydrol.2010.03.027.

J. H. Blöthe and O. Korup. Millennial lag times in the himalayan sediment routing system. *Earth and Planetary Science Letters*, 382:38–46, 2013.

T. Chakraborty, R. Kar, P. Ghosh, and S. Basu. Kosi megafan: Historical records, geomorphology and the recent avulsion of the Kosi River. *Quaternary International*, 227(2):143–160, 2010. ISSN 10406182. doi: 10.1016/j.quaint.2009.12.002. URL http://dx.doi.org/10.1016/j.quaint.2009.12.002.

T. Coulthard and M. Macklin. How sensitive are river systems to climate and land-use changes? a model-based evaluation. *Journal of Quaternary Science: Published for the Quaternary Research Association*, 16(4):347–351, 2001.

T. Coulthard and M. Van De Wiel. 9.34 Numerical Modeling in Fluvial Geomorphology. In *Treatise on Geomorphology*, volume 9, pages 694–710. Elsevier, 2013. ISBN 9780080885223. doi: 10.1016/B978-0-12-374739-6.00261-X. URL http://dx.doi.org/10.1016/B978-0-12-374739-6.00261-Xhttps://linkinghub.elsevier.com/retrieve/pii/B978012374739600261X.

T. Coulthard, M. Kirkby, and M. Macklin. Modelling hydraulic, sediment transport and slope processes, at a catchment scale, using a cellular automaton approach. In *Proceedings of the 2nd Annual Conference: GeoComputation*, volume 97, pages 309–318, 1997.

T. Coulthard, M. Macklin, and M. Kirkby. A cellular model of holocene upland river basin and alluvial fan evolution. *Earth Surface Processes and Landforms*, 27(3):269–288, 2002.

T. J. Coulthard and M. G. Macklin. Modeling long-term contamination in river systems from historical metal mining. *Geology*, 31(5):451–454, 2003.

T. J. Coulthard and M. J. Van De Wiel. Modelling long term basin scale sediment connectivity, driven by spatial land use changes. *Geomorphology*, 277:265–281, 2017. ISSN 0169555X. doi: 10.1016/j.geomorph.2016.05.027. URL http://dx.doi.org/10.1016/j.geomorph.2016.05.027.

T. J. Coulthard and M. J. V. D. Wiel. A cellular model of river meandering. *Earth Surface Processes and Landforms: The Journal of the British Geomorphological Research Group*, 31 (1):123–132, 2006. ISSN 01979337. doi: 10.1002/esp.1315.

T. J. Coulthard, D. M. Hicks, and M. J. Van De Wiel. Cellular modelling of river catchments and reaches: Advantages, limitations and prospects. *Geomorphology*, 90(3-4):192–207, 2007. ISSN 0169555X. doi: 10.1016/j.geomorph.2006.10.030.

T. J. Coulthard, J. C. Neal, P. D. Bates, J. Ramirez, G. A. de Almeida, and G. R. Hancock. Integrating the LISFLOOD-FP 2D hydrodynamic model with the CAESAR model: Implications for modelling landscape evolution. *Earth Surface Processes and Landforms*, 38(15): 1897–1906, 2013. ISSN 10969837. doi: 10.1002/esp.3478.

T. J. T. Coulthard, J. Lewin, and M. G. Macklin. Modelling differential catchment response to environmental change. *Geomorphology*, 69:222–241, 2005. doi: 10.1016/j.geomorph.2005.01.008.

R. K. Dahal and S. Hasegawa. Representative rainfall thresholds for landslides in the nepal himalaya. *Geomorphology*, 100(3-4):429–443, 2008.

T. H. Dewan. Societal impacts and vulnerability to floods in bangladesh and nepal. *Weather and Climate Extremes*, 7:36–42, 2015.

Y. Dhital and R. Kayastha. Frequency analysis, causes and impacts of flooding in the b agmati r iver b asin, n epal. *Journal of Flood Risk Management*, 6(3):253–260, 2013.

E. Dingle, M. Creed, H. Sinclair, D. Gautam, N. Gourmelen, A. Borthwick, and M. Attal. Dynamic flood topographies in the terai region of nepal. *Earth Surface Processes and Landforms*, 45(13):3092–3102, 2020.

H. A. Einstein. *The bed-load function for sediment transportation in open channel flows*. US Department of Agriculture, 1950.

D. G. Emerson, A. V. Vecchia, and A. L. Dahl. *Evaluation of drainage-area ratio method used to estimate streamflow for the Red River of the North Basin, North Dakota and Minnesota*. US Department of the Interior, US Geological Survey Reston, VA, USA, 2005.

T. G. Farr, P. A. Rosen, E. Caro, R. Crippen, R. Duren, S. Hensley, M. Kobrick, M. Paller, E. Rodriguez, L. Roth, D. Seal, S. Shaffer, J. Shimada, J. Umland, M. Werner, M. Oskin, D. Burbank, and D. Alsdorf. The shuttle radar topography mission. *Reviews of Geophysics*, 45(2):RG2004, May 2007. ISSN 8755-1209. doi: 10.1029/2005RG000183.

C. J. Feeney, R. C. Chiverrell, H. G. Smith, J. M. Hooke, and J. R. Cooper. Modelling the decadal dynamics of reach-scale river channel evolution and floodplain turnover in CAESAR-Lisflood. *Earth Surface Processes and Landforms*, 45(5):1273–1291, 4 2020. ISSN 0197-9337. doi: 10.1002/esp.4804. URL https://onlinelibrary.wiley.com/doi/10.1002/esp.4804.

D. M. Fieman, M. Attal, and S. Addy. Geomorphic response of a mountain gravel-bed river to an extreme flood in aberdeenshire, scotland. *Scottish Journal of Geology*, 56(2):101–116, 2020. ISSN 00369276. doi: 10.1144/sjg2019-005.

GoN. Develop an Information Base and Strategies for Environmental Improvement of Bagmati River and Its Territory. Technical report, Adhikar Sampanna Bagmati Sabhyata Akirit Samitee and UN-HABITAT, Water for Asian Cities Programme, Nepal, 2008.

M. Guan, N. G. Wright, and P. A. Sleigh. Multiple effects of sediment transport and geomorphic processes within flood events: Modelling and understanding. *International Journal of Sediment Research*, 30(4):371–381, 2015. ISSN 10016279. doi: 10.1016/j.ijsrc.2014.12.001.

M. Guan, J. L. Carrivick, N. G. Wright, P. A. Sleigh, and K. E. H. Staines. Quantifying the combined effects of multiple extreme floods on river channel geometry and on flood hazards. *Journal of Hydrology*, 538:256–268, 2016. ISSN 0022-1694. doi: 10.1016/j.jhydrol.2016.04.004. URL http://dx.doi.org/10.1016/j.jhydrol.2016.04.004.

N. Gurung, M. Fort, R. Bell, G. Arnaud-Fassetta, and N. R. Maharjan. Hydro-torrential hazard vs. anthropogenic activities along the seti valley, kaski, nepal: Assessment and recommendations from a risk perspective. *Journal of Nepal Geological Society*, 62:58–87, 2021.

G. Hancock. A catchment scale assessment of increased rainfall and storm intensity on erosion and sediment transport for northern australia. *Geoderma*, 152(3-4):350–360, 2009.

G. Hancock. Modelling stream sediment concentration: An assessment of enhanced rainfall and storm frequency. *Journal of Hydrology*, 430:1–12, 2012.

Y. Hirabayashi, R. Mahendran, S. Koirala, L. Konoshima, D. Yamazaki, S. Watanabe, H. Kim, and S. Kanae. Global flood risk under climate change. *Nature climate change*, 3(9):816–821, 2013.

IH. Handbook, flood estimation. *Institute of Hydrology, Wallingford, UK*, 1999.

IPCC. *Summary for policymakers. In: Parry, M.L., Canziani, O.F., Palutikof, J.P., van der Linden, P.J., Hanson, C.E. (Eds.),Climate Change 2007: Impacts, Adaptation and Vulnerability. Contribution of Working Group II to the Fourth Assessment Report of the Intergovernmental Panel on Climate Change.*, volume 4. Cambridge University Press, 2007.

S. N. Lane, V. Tayefi, S. C. Reid, D. Yu, and R. J. Hardy. Interactions between sediment delivery , channel change , climate change and flood risk in a temperate upland environment. *Earth Surface Processes and Landforms*, 32:429–446, 2007. doi: 10.1002/esp.1404.

B. Liu and T. J. Coulthard. Modelling the interaction of aeolian and fluvial processes with a combined cellular model of sand dunes and river systems. *Computers & Geosciences*, 106: 1–9, 2017.

M. Lupker, P.-H. Blard, J. Lavé, C. France-Lanord, L. Leanni, N. Puchol, J. Charreau, and D. Bourlès. 10be-derived himalayan denudation rates and sediment budgets in the ganga basin. *Earth and Planetary Science Letters*, 333:146–156, 2012.

B. Maharjan and N. K. Tamrakar. Morpho-hydraulic parameters and existing stability condition of nakhu river, southern kathmandu, central nepal. *Bulletin of the Department of Geology*, 13:1–12, 2010.

B. Maharjan and N. K. Tamrakar. Deterioration of the nakhu river: impairment on dynamic and recreational functions of the river. *Journal of Nepal Geological Society*, 43:225–240, 2011.

S. Marahatta, L. Devkota, and D. Aryal. Hydrological modeling: a better alternative to empirical methods for monthly flow estimation in ungauged basins. *Journal of Water Resource and Protection*, 13(3):254–270, 2021.

V. Masson-Delmotte, P. Zhai, A. Pirani, S. Connors, C. Péan, S. Berger, N. Caud, Y. Chen, L. Goldfarb, M. Gomis, M. Huang, K. Leitzell, E. Lonnoy, J. Matthews, T. Maycock, T. Waterfield, O. Yelekçi, R. Yu, and B. Z. (eds.). Summary for policymakers. in: Climate change

2021: The physical science basis. contribution of working group i to the sixth assessment report of the intergovernmental panel on climate change. Technical report, IPCC, UNEP, 2021. URL https://www.ipcc.ch/report/ar6/wg1/chapter/summary-for-policymakers/.

T. Meadows. *Forecasting long-term sediment yield from the upper North Fork Toutle River, Mount St. Helens, USA*. PhD thesis, University of Nottingham, 2014.

E. Meyer-Peter and R. Müller. Formulas for bed-load transport. In *IAHSR 2nd meeting, Stockholm, appendix 2*. IAHR, 1948.

D. J. Milan and A. C. Schwendel. Climate-change driven increased flood magnitudes and frequency in the british uplands: geomorphologically informed scientific underpinning for upland flood-risk management. *Earth Surface Processes and Landforms*, 46(15):3026–3044, 2021.

J. R. Miller and J. M. Friedman. Influence of flow variability on floodplain formation and destruction, Little Missouri River, North Dakota. *Geological Society of America Bulletin*, 121 (5-6):752–759, 5 2009. ISSN 0016-7606. doi: 10.1130/B26355.1. URL http://gsabulletin.gsapubs.org/cgi/doi/10.1130/B26355.1.

J. D. Milliman and R. H. Meade. World-wide delivery of river sediment to the oceans. *The Journal of Geology*, 91(1):1–21, 1983.

G. P. Morin, J. Lavé, C. France-Lanord, T. Rigaudier, A. P. Gajurel, and R. Sinha. Annual sediment transport dynamics in the narayani basin, central nepal: assessing the impacts of erosion processes in the annual sediment budget. *Journal of Geophysical Research: Earth Surface*, 123(10):2341–2376, 2018.

C. Neuhold, P. Stanzel, and H. Nachtnebel. Incorporating river morphological changes to flood risk assessment: uncertainties, methodology and application. *Natural Hazards and Earth System Sciences*, 9(3):789–799, 2009.

J. E. O'Connor, M. A. Jones, and T. L. Haluska. Flood plain and channel dynamics of the quinault and queets rivers, washington, usa. *Geomorphology*, 51(1-3):31–59, 2003.

P. N. Owens and A. J. Collins. Soil erosion and sediment redistribution in river catchments: Measurement, modelling and management. *Soil Erosion and Sediment Redistribution in River Catchments: Measurement, Modelling and Management*, pages 1–328, 2006. doi: 10.1079/9780851990507.0000.

N. Pinter and R. A. Heine. Hydrodynamic and morphodynamic response to river engineering documented by fixed-discharge analysis, lower missouri river, usa. *Journal of Hydrology*, 302 (1-4):70–91, 2005.

B. Pratt-Sitaula, M. Garde, D. W. Burbank, M. Oskin, A. Heimsath, and E. Gabet. Bedload-to-suspended load ratio and rapid bedrock incision from himalayan landslide-dam lake record. *Quaternary Research*, 68(1):111–120, 2007.

J. A. Ramirez, A. P. Zischg, S. Schürmann, M. Zimmermann, R. Weingartner, T. Coulthard, and M. Keiler. Modeling the geomorphic response to early river engineering works using CAESAR-Lisflood. *Anthropocene*, 32:100266, 12 2020. ISSN 22133054. doi: 10.1016/j.ancene.2020.100266. URL https://linkinghub.elsevier.com/retrieve/pii/S2213305420300321.

J. A. Ramirez, M. Mertin, N. Peleg, P. Horton, C. Skinner, M. Zimmermann, and M. Keiler. Modelling the long-term geomorphic response to check dam failures in an alpine channel with CAESAR-Lisflood. *International Journal of Sediment Research*, 37(5):687–700, 2022. ISSN 10016279. doi: 10.1016/j.ijsrc.2022.04.005. URL https://doi.org/10.1016/j.ijsrc.2022.04.005.

V. Ruiz-Villanueva, S. Allen, M. Arora, N. K. Goel, and M. Stoffel. Recent catastrophic landslide lake outburst floods in the himalayan mountain range. *Progress in Physical Geography*, 41(1):3–28, 2017.

G. H. Sambrook Smith and A. P. Nicholas. Effect on flow structure of sand deposition on a gravel bed: Results from a two-dimensional flume experiment. *Water Resources Research*, 41(10), 2005.

B. B. Shrestha and H. Nakagawa. Hazard assessment of the formation and failure of the sunkoshi landslide dam in nepal. *Natural Hazards*, 82:2029–2049, 2016.

D. Shrestha, D. B. Basnyat, J. Gyawali, M. J. Creed, H. D. Sinclair, B. Golding, M. Muthusamy, S. Shrestha, D. L. Subedi, R. Haiju, and S. C. Watson. Rainfall extremes under future climate change with implications for urban flood risk in kathmandu, nepal. forthcoming, 2023.

C. J. Skinner and T. J. Coulthard. Testing the sensitivity of the caesar-lisflood landscape evolution model to grid cell size. *Earth Surface Dynamics*, 11(4):695–711, 2023. doi: 10.5194/esurf-11-695-2023. URL https://esurf.copernicus.org/articles/11/695/2023/.

C. J. Skinner, T. J. Coulthard, W. Schwanghart, M. J. Van De Wiel, and G. Hancock. Global sensitivity analysis of parameter uncertainty in landscape evolution models. *Geoscientific Model Development*, 11(12):4873–4888, 12 2018. ISSN 1991-9603. doi: 10.5194/gmd-11-4873-2018. URL https://gmd.copernicus.org/articles/11/4873/2018/.

L. J. Slater, M. B. Singer, and J. W. Kirchner. Hydrologic versus geomorphic drivers of trends in flood hazard. *Geophysical Research Letters*, 42(2):370–376, 2015.

M. Stoffel, B. Wyżga, and R. A. Marston. Floods in mountain environments: A synthesis. *Geomorphology*, 272:1–9, 2016. ISSN 0169555X. doi: 10.1016/j.geomorph.2016.07.008.

S. C. Stover and D. R. Montgomery. Channel change and flooding, Skokomish River, Washington. *Journal of Hydrology*, 243(3-4):272–286, 2001. ISSN 00221694. doi: 10.1016/S0022-1694(00)00421-2.

A. Temme, L. Claessens, A. Veldkamp, and J. Schoorl. Evaluating choices in multi-process landscape evolution models. *Geomorphology*, 125(2):271–281, 2011.

S. Thapa, A. Shrestha, S. Lamichhane, R. Adhikari, and D. Gautam. Catchment-scale flood hazard mapping and flood vulnerability analysis of residential buildings: The case of Khando River in eastern Nepal. *Journal of Hydrology: Regional Studies*, 30(March):100704, 2020. ISSN 22145818. doi: 10.1016/j.ejrh.2020.100704. URL https://doi.org/10.1016/j.ejrh.2020.100704.

S. Thapa, M. Creed, H. Sinclair, S. Mudd, M. Attal, M. Muthusamy, and B. N. Ghimire. Modelling the impact of sediment grain size on flooding in the kathmandu basin, nepal. In *39th IAHR World Congress: From Snow to Sea*, pages 784–794. International Association for Hydro-Environment Engineering and Research (IAHR), 2022.

J. M. Turowski, E. M. Yager, A. Badoux, D. Rickenmann, and P. Molnar. The impact of exceptional events on erosion, bedload transport and channel stability in a step-pool channel. *Earth Surface Processes and Landforms*, 34(12):1661–1673, 2009.

J. M. Turowski, D. Rickenmann, and S. J. Dadson. The partitioning of the total sediment load of a river into suspended load and bedload: a review of empirical data. *Sedimentology*, 57 (4):1126–1146, 2010.

UNDRR. United Nations Office for Disaster Risk Reduction. *The human cost of disasters: an overview of the last 20 years (2000-2019), United Nations Office for Disaster Risk Reduction*, 2020.

D. A. Valters. *Modelling catchment sensitivity to rainfall resolution and erosional parameterisation in simulations of flash floods in the UK*. The University of Manchester (United Kingdom), 2017.

M. J. Van De Wiel and T. J. Coulthard. Self-organized criticality in river basins: Challenging sedimentary records of environmental change. *Geology*, 38(1):87–90, 2010. ISSN 00917613. doi: 10.1130/G30490.1.

M. J. Van De Wiel, T. J. Coulthard, M. G. Macklin, and J. Lewin. Embedding reach-scale fluvial dynamics within the CAESAR cellular automaton landscape evolution model. *Geomorphology*, 90(3-4):283–301, 10 2007. ISSN 0169555X. doi: 10.1016/j.geomorph.2006.10.024. URL https://linkinghub.elsevier.com/retrieve/pii/S0169555X07001341.

M. J. Van De Wiel, T. J. Coulthard, M. G. Macklin, and J. Lewin. Modelling the response of river systems to environmental change: Progress, problems and prospects for palaeo-environmental reconstructions. *Earth-Science Reviews*, 104(1-3):167–185, 2011. ISSN 00128252. doi: 10.1016/j.earscirev.2010.10.004. URL http://dx.doi.org/10.1016/j.earscirev.2010.10.004.

P. R. Wilcock and J. C. Crowe. Surface-based transport model for mixed-size sediment. *Journal of hydraulic engineering*, 129(2):120–128, 2003.

J. S. Wong, J. E. Freer, P. D. Bates, J. Warburton, and T. J. Coulthard. Assessing the hydrological and geomorphic behaviour of a landscape evolution model within a limits-of-acceptability uncertainty analysis framework. *Earth Surface Processes and Landforms*, 46(10):1981–2003, 8 2021. ISSN 0197-9337. doi: 10.1002/esp.5140. URL https://onlinelibrary.wiley.com/doi/10.1002/esp.5140.

E. Yager, J. Turowski, D. Rickenmann, and B. McArdell. Sediment supply, grain protrusion, and bedload transport in mountain streams. *Geophysical Research Letters*, 39(10), 2012.

M. U. Yilmaz and B. Onoz. A comparative study of statistical methods for daily streamflow estimation at ungauged basins in turkey. *Water*, 12(2):459, 2020.

L. Ziliani, N. Surian, T. Coulthard, and S. Tarantola. Reduced-complexity modeling of braided rivers: Assessing model performance by sensitivity analysis, calibration, and validation. *Journal of Geophysical Research: Earth Surface*, 118(4):2243–2262, 2013.

L. Ziliani, N. Surian, G. Botter, and L. Mao. Assessment of the geomorphic effectiveness of controlled floods in a braided river using a reduced-complexity numerical model. *Hydrology and Earth System Sciences*, 24(6):3229–3250, 2020. ISSN 16077938. doi: 10.5194/hess-24-3229-2020.